Semaphorin 3A is an endogenous angiogenesis inhibitor that blocks tumor growth and normalizes tumor vasculature in transgenic mouse models

Federica Maione,[1,2] Fabiola Molla,[3] Claudia Meda,[1,2] Roberto Latini,[3] Lorena Zentilin,[4] Mauro Giacca,[4] Giorgio Seano,[1,2] Guido Serini,[1,2,5] Federico Bussolino,[1,2,5] and Enrico Giraudo[1,2,5]

[1]Department of Oncological Sciences, University of Torino School of Medicine, Candiolo, Italy. [2]Division of Vascular Biology, Institute for Cancer Research and Treatment (IRCC), University of Torino School of Medicine, Candiolo, Italy. [3]Cardiovascular Clinical Pharmacology Laboratory, Mario Negri Institute for Pharmacological Research, Milan, Italy. [4]Molecular Medicine Laboratory, International Centre for Genetic Engineering and Biotechnology (ICGEB), Trieste, Italy. [5]Center for Complex Systems in Molecular Biology and Medicine (SysBioM), University of Torino, Turin, Italy.

Tumor growth and progression rely upon angiogenesis, which is regulated by pro- and antiangiogenic factors, including members of the semaphorin family. By analyzing 3 different mouse models of multistep carcinogenesis, we show here that during angiogenesis, semaphorin 3A (Sema3A) is expressed in ECs, where it serves as an endogenous inhibitor of angiogenesis that is present in premalignant lesions and lost during tumor progression. Pharmacologic inhibition of endogenous Sema3A during the angiogenic switch, the point when pretumoral lesions initiate an angiogenic phase that persists throughout tumor growth, enhanced angiogenesis and accelerated tumor progression. By contrast, when, during the later stages of carcinogenesis following endogenous Sema3A downmodulation, Sema3A was ectopically reintroduced into islet cell tumors by somatic gene transfer, successive waves of apoptosis ensued, first in ECs and then in tumor cells, resulting in reduced vascular density and branching and inhibition of tumor growth and substantially extended survival. Further, long-term reexpression of Sema3A markedly improved pericyte coverage of tumor blood vessels, something that is thought to be a key property of tumor vessel normalization, and restored tissue normoxia. We conclude, therefore, that Sema3A is an endogenous and effective antiangiogenic agent that stably normalizes the tumor vasculature.

Introduction

The natural history of solid cancers is characterized by the initial formation of microscopic avascular lesions that must promote the development of new blood vessels, i.e., angiogenesis, in order to grow beyond a minimal size and metastasize in host tissues (1). Cancer neovascularization is thought to be regulated by a balance between pro- and antiangiogenic factors (2) whose molecular identity, reciprocal interactions, and physiopathological role are not yet fully outlined. The stimulatory role of VEGF-A and its receptor VEGFR2 in tumor angiogenesis has been clearly proven over the years (1–3), and these molecules therefore appeared to be ideal targets for antiangiogenic therapy (4). However, preclinical (5) and clinical trials (4) recently showed that cancer can develop resistance to anti-VEGF therapy, likely because of the induction of other proangiogenic factors, such as bFGF (5) and the VEGF homolog placental growth factor (PlGF) (6). Hence, there is presently a mounting requirement to identify and characterize additional molecular regulators of angiogenesis. Notably, the fact that tumor blood vessels function poorly and display structural defects (2) that are normalized by treatment with anti-VEGF Abs offers a rationale for the observed synergistic effect between VEGF blockade and conventional cancer therapies (2, 4, 7) and suggests that in tumors, the activity of angiogenic stimulators somehow overrides that of endogenous inhibitors (2). Therefore, investigating the role played by endogenous antiangiogenic factors during cancer progression could help in identifying new pharmacological targets.

Since early anatomical studies in the fifteenth century, it has been known that vascular and neural networks are architecturally similar and interact physically (8). Nevertheless, only in the last decade did it come to light that blood vessels and nerves are guided in their journey through the body by the same families of cues (8, 9). Among these cues, secreted chemorepulsive class 3 semaphorins (Sema3) have been the molecules most clearly involved in both physiological and tumor angiogenesis (10–16). Neuropilin 1 and 2 (Nrp1 and Nrp2) and the type A/D plexins (Plxns) act as the ligand binding and the signal transducing subunits of Sema3 receptor complexes on the surface of ECs (17). Additionally, the activity of the proangiogenic factor VEGF-A is modulated by interactions with Nrps in addition to its canonical tyrosine kinases VEGFR-1 and -2 (11). In particular, in embryo development, Sema3A mainly takes part in the late phase of angiogenesis, characterized by the remodeling of the primitive plexus into a mature vascular tree (10). Indeed, Sema3A and Sema3F, respectively acting via Nrp1 and Nrp2, trigger inhibitory signaling pathways that negatively regulate integrin-mediated adhesion of cultured ECs (10, 11, 15, 18) and experimental angiogenesis in vivo (11–13, 16). Moreover, mutually antagonistic autocrine loops of VEGF-A and Sema3 are present in ECs both in vitro (10, 14, 19) and during normal angiogenic remodeling in

Authorship note: Guido Serini, Federico Bussolino, and Enrico Giraudo contributed equally to this work.

Conflict of interest: The authors have declared that no conflict of interest exists.

Citation for this article: *J. Clin. Invest.* **119**:3356–3372 (2009). doi:10.1172/JCI36308.

vivo (10, 20). Therefore, an imbalance in the ratio of autocrine VEGF-A to Sema3 in ECs could occur during tumor progression and account at least in part for the structural and functional abnormalities of tumor vasculature (2). This hypothesis is further strengthened by the observation that in bone marrow ECs of patients with malignant multiple myeloma, autocrine loops of Sema3A are lost in favor of VEGF-A (14).

Recently, it was shown that — in addition to Sema3A and Sema3F — Sema3D, Sema3E, and Sema3G repel cultured ECs, reduce the density of blood vessels, and inhibit the growth of tumor xenografts (21). In contrast, furin-dependent cleavage of full-length Sema3E gives rise to a 61-kDa isoform that promotes EC migration and tumor metastasis (22), and Sema3B, while inhibiting cancer growth, favors metastasis via the IL-8–mediated recruitment of tumor-associated macrophages (23). Therefore, semaphorins can display complex behavior in regulating tumor angiogenesis, growth, and metastatic dissemination.

Transgenic mouse models of multistage tumorigenesis, such as RipTag2 and HPV/E_2 mice, have been found to generically recapitulate the progressive development of human cancers. Indeed, both of these genetically engineered mouse models are characterized by an angiogenic phase that switches on in pretumoral stages and then persists throughout tumor growth (24). RipTag2 mice express SV40 T antigen oncogenes under the control of insulin promoter and develop islet cell carcinomas (25). In addition, the keratin 14 (K14) promoter–driven expression of the human papilloma virus type 16 (HPV16) early gene results in squamous cell carcinomas (SCCs) of K14-HPV16 mice (26). When K14-HPV16 females are implanted with 17β-estradiol (estrogen [E_2]) capsules to sustain the estrus phase (i.e., HPV/E_2 mice), a synchronous progression leading to invasive uterine cervical cancer ensues (27, 28). Importantly, in RipTag2 mice, while VEGF-A has been found to be crucial for angiogenesis (3), in late-stage tumors a resistance to VEGF-A blockade came to light, which was due at least in part to hypoxia-driven induction of proangiogenic factors (5). However, we speculated that loss of endogenous angiogenesis inhibitors such as Sema3 during cancer progression could play a crucial role as well. Therefore, we sought to investigate Sema3 ligands and their receptors during multiphase progression and angiogenesis of tumors developing in RipTag2, K14-HPV16, and HPV/E_2 mouse models.

Results

Sema3s and their receptor complexes are modulated during tumor progression. To assess the role of Sema3s, Nrps, and Plxns in regulating tumor angiogenesis, we profiled their gene expression through neoplastic progression in mouse models of pancreatic β cell (RipTag2), cervical (HPV/E_2), and skin (K14-HPV16) tumorigenesis. RipTag2 tumors develop from oncogene-expressing normal islets in pancreas through successive stages, i.e., hyperplastic islets, angiogenic islets, and tumors, which were compared with nontransgenic normal islets (29). HPV/E_2 mice develop cervical cancer through progression from low-grade cervical intraepithelial neoplasia (CIN-1/2), to high-grade dysplasia (CIN-3), and then to cervical SCC lesions compared with nontransgenic E_2-treated normal cervix (28). In K14-HPV16 mice, skin hyperplasias progress to dysplasias and in turn to SCC, which were compared with nontransgenic normal skin (26). Real-time RT-PCR revealed that *Sema3a*, *Sema3f*, and, to a lesser extent, *Sema3e* transcripts were highly upregulated in the dysplastic/angiogenic stages (CIN-3 and dysplasias) compared with the normal conditions, but then strongly downmodulated in tumors (SCC) compared with both normal and dysplastic tissues. In contrast, in all 3 mouse models, *Sema3b*, *Sema3c*, and *Sema3d* mRNA expression was inhibited through all the stages. Finally, in all 3 tumor types, *Sema3g*, a new member of the Sema3 family that repels ECs and inhibit tumor angiogenesis (21), was slightly upregulated in the dysplastic stages and in tumors compared with normal tissues (Figure 1, A and B, and Supplemental Figure 1A; supplemental material available online with this article; doi:10.1172/JCI36308DS1). The expression of both *Nrp1* and *Nrp2* mRNA was similarly upregulated in both dysplastic lesions and in tumors compared with normal tissues (Figure 1, C and D, and Supplemental Figure 1B), supporting their possible involvement in tumor angiogenesis and growth (11, 30). Among the several *Plxn* genes studied, *Plxna1* and *Plxna2* transcription was significantly modulated through tumor progression. While in all 3 models, *Plxna1* mRNA increased in angiogenic islets, CIN-3, dysplasias, and tumor stages, *Plxna2* expression increased in dysplasia and declined in tumors, thus paralleling the expression of *Sema3a* and *Sema3f*. Notably, the Sema3A and Sema3F signaling receptor subunits (9) PlxnA1 and PlxnA2 are known to be expressed in ECs (31, 32). Finally, *Plxnd1*, an endothelial Sema3 receptor (9) that is induced in the tumor vasculature (33), and *Plxnb1*, which conveys Sema4D angiogenic signaling in ECs (9), were upregulated in both the dysplastic and tumor stages (Figure 1, E and F, and Supplemental Figure 1C). Moreover, by ELISA we detected very similar protein expression patterns of the most modulated Sema3, Nrp, and PlxnA and -D genes through the stages of RipTag2 tumorigenesis (Supplemental Figure 2). Since we did not observe statistically significant differences in *Sema3*, *Nrp*, or *Plxn* expression in the (largely preangiogenic) hyperplastic stages compared with controls (Figure 1 and Supplemental Figure 1), we focused our subsequent analysis on the normal, angiogenic-dysplastic, and tumor stages. Furthermore, since our analysis showed that the transcription profile of genes encoding Sema3A, Sema3F, and their receptors is similar in 3 different models of cancer progression, we sought to investigate the hypothesis that they were involved in the regulation of tumor angiogenesis and growth in these tumorigenesis models.

Sema3A and Sema3F are expressed by different cell types during tumor progression. To begin clarifying whether Sema3A and Sema3F proteins might play a role in tumorigenesis, we examined their expression patterns in the cell types composing the lesional microenvironments of the different stages of the 3 models. Sema3A was highly expressed in ECs and to a lesser extent in epithelium of angiogenic islets in RipTag2 mice, while it was barely detectable in tumors (Figure 2A). Sema3A was also present in few scattered ECs of normal vessels and in the normal epithelium (Figure 2A). Similar results were obtained in HPV/E_2 mice, where vascular ECs, basal squamous epithelial cells, and a subset of macrophages of CIN-3 cervix lesions synthesized high amounts of Sema3A (Figure 2B and Supplemental Figure 4A). The expression pattern of Sema3A in skin lesions of K14-HPV16 mice was similar to that of the cervical lesions of HPV/E_2 mice (data not shown). While ECs did not express Sema3F in any stage of insulinoma progression, the epithelium of normal RipTag2 islets produced Sema3F that in the angiogenic phase was upregulated in dysplastic epithelial cells and completely suppressed in tumor cells (Supplemental Figure 3A). Likewise, in

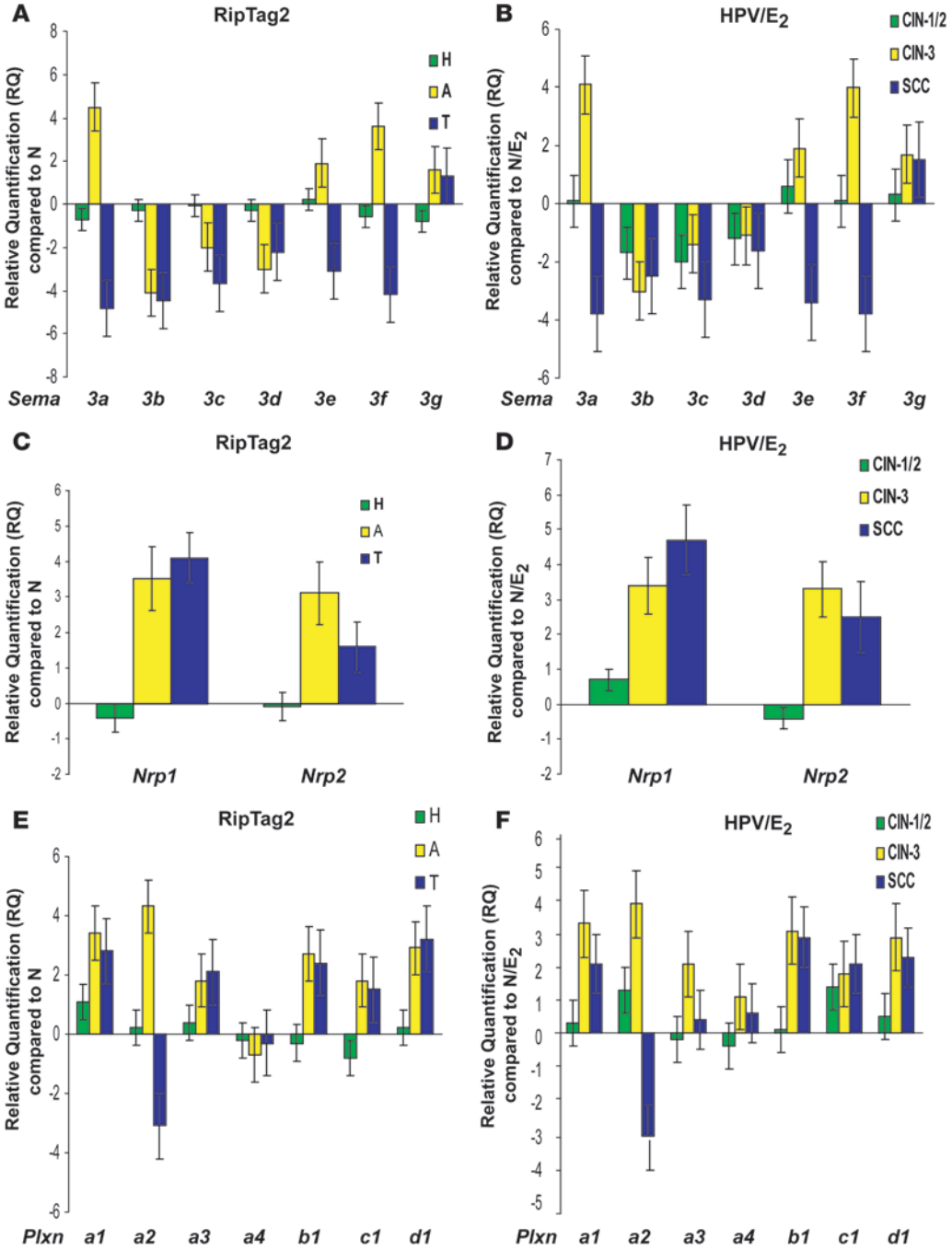

Figure 1

Gene expression profile of Sema3s and their receptors during RipTag2 and HPV/E_2 tumorigenesis. (**A** and **B**) Real-time RT-PCR revealed that *Sema3a, Sema3f*, and, to a lesser extent, *Sema3e* transcripts were strongly upregulated both in angiogenic islets (A) of RipTag2 mice (**A**) and in CIN-3 of HPV/E_2 mice (**B**) and downregulated in tumors (T) and SCC, as compared with normal islets (N) and E_2-treated normal cervix (N/E2), respectively. (**C** and **D**) Compared with that in normal stages, *Nrp1* and *Nrp2* expression increased in both angiogenic islets and tumors (**C**) as well as in CIN-3 and SCC (**D**). (**E** and **F**) Compared with that in normal islets and E_2-treated normal cervix, *Plxna1, Plxnd1*, and *Plxnb1* mRNA was upregulated in both angiogenic islets and tumors (**E**) in addition to CIN-3 and SCC (**F**). In contrast, *Plxna2* transcript increased in angiogenic islets and CIN-3 and decreased in tumors and SCC. Normalized relative quantification (RQ) values are compared with normal stages and are mean ± SD of 4 experiments. Sema3A transcript was present in sizeable amounts (pg per 100 ng of total RNA) in normal islets (Sema3A, 46 pg) and in normal cervix (Sema3A, 53 pg; see Supplemental Methods). Values were normalized to the endogenous *Gus* housekeeping gene. Total RNA derived from pools of islets or tissue lesions of 10 mice per stage (20 mice for normal islets). H, hyperplastic islets; CIN-1, -2, and -3, low, moderate, and high CIN, respectively.

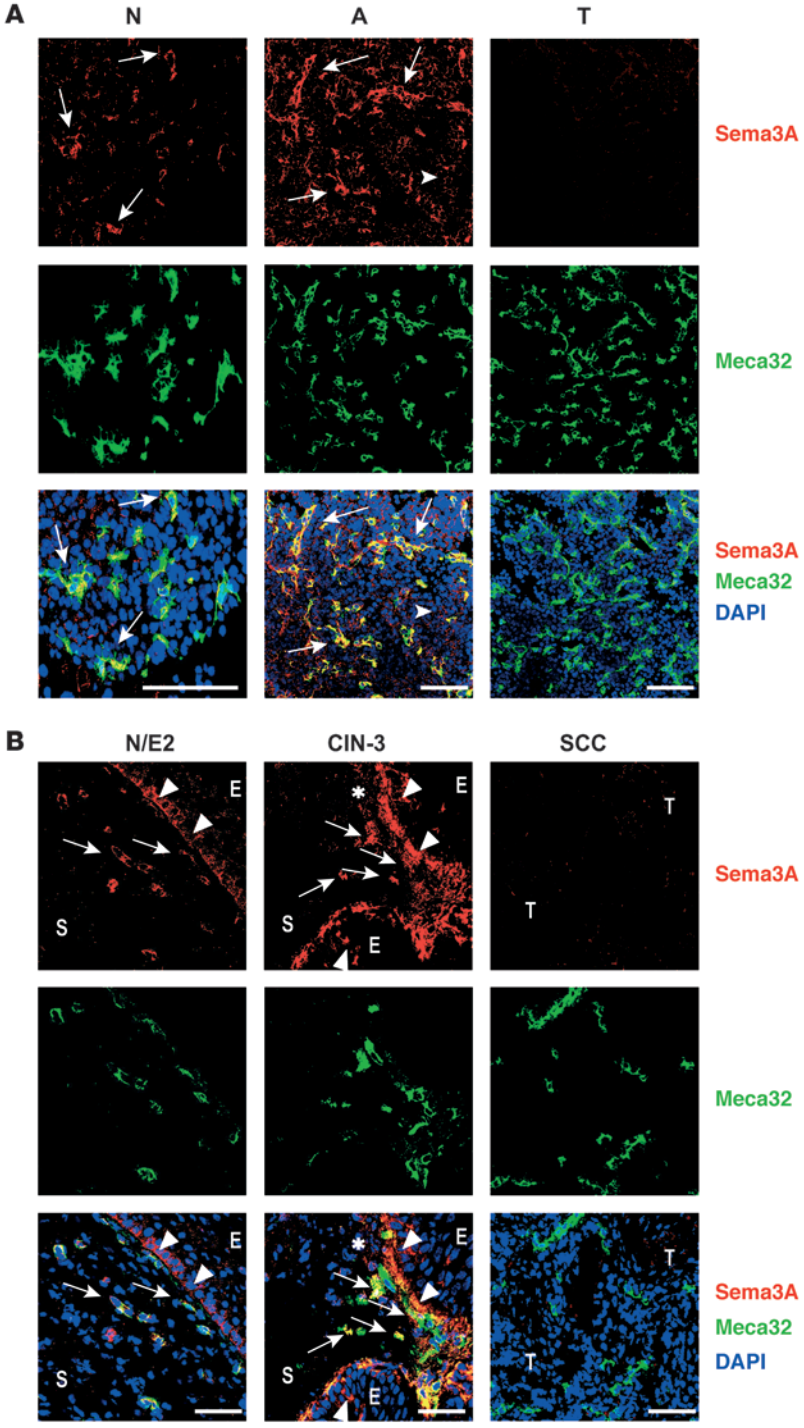

Figure 2
Cell type–specific localization of Sema3A during RipTag2 and HPV/E_2 tumor progression. (**A**) Fluorescence confocal microscopy of RipTag2 mice using an anti-Sema3A Ab (red) revealed Sema3A expression in vessels (arrows) and epithelium of normal islets; Sema3A was highly expressed in angiogenic islets (arrows) and absent in tumors. Sema3A was mainly expressed by ECs, as revealed by colocalization of Meca-32 (green) with Sema3A (red) (arrows); Sema3A was present to a lesser extent in dysplastic epithelium (arrowheads). (**B**) In HPV/E_2 mice, Sema3A (red) was expressed in Meca-32–positive (green) blood vessels (arrows) and in the squamous epithelium (arrowheads) of E_2-treated normal cervix and CIN-3 lesions. Sema3A was also detected in scattered cells in the stroma underlying CIN-3 lesions (asterisks). Sema3A was barely detectable in SCC. Confocal analysis was performed on tissue sections from 10 mice per stage of both models and images are representative of 5 fields observed per stages. E, epithelium; S, stroma; Scale bars: 50 μm.

HPV/E_2 mice, Sema3F was expressed in basal epithelial cells of normal tissue, upregulated in squamous epithelium of the CIN-3 stage, and downmodulated in SCC. Furthermore, Sema3F was also localized in a subset of vessels and in perivascular cells near CIN-3 lesions (Supplemental Figure 3B and Supplemental Figure 4B). Analogous observations were made in the skin of K14-HPV16 mice (data not shown).

Fluorescence confocal microscopy revealed that through the different stages of RipTag2 tumorigenesis the amount of Nrp1, Nrp2, PlxnA1, and PlxnA2 proteins was modulated in accordance with the gene expression analysis (Supplemental Figures 5 and 6).

In summary, our gene expression and protein analysis showed that Sema3A and Sema3F are the most significantly modulated Sema3s in all 3 different models of cancer progression we studied. The role of Sema3F has been thoroughly investigated by others (12, 15, 21), while the function of Sema3A during spontaneous carcinogenesis is still unclear. Hence, we chose to specifically focus our studies on the role of Sema3A in tumor angiogenesis.

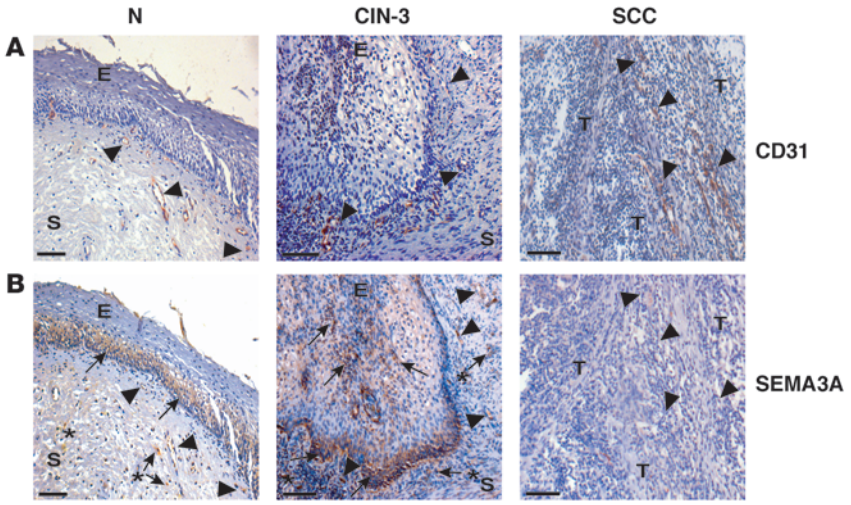

Figure 3
SEMA3A expression during human uterine cervical cancer progression. (**A**) Blood vessels were detected by immunohistochemical analysis employing a CD31 Ab. (**B**) SEMA3A was present in some blood vessels in normal cervix (N) (arrowheads) and in the basal squamous epithelium (arrows); SEMA3A was expressed at high levels in vessels proximal to CIN-3 lesions (arrowheads), in squamous epithelium (arrows), and in scattered stromal cells (asterisks). Notably SEMA3A was barely detectable in SCC. SEMA3A expression was evaluated by immunostaining utilizing anti-SEMA3A Ab in parallel to CD31 analysis in consecutive sections. These images are representative of experiments repeated 3 times; 12 different samples per stage and 5 fields per sample were evaluated. Scale bars: 50 μm.

SEMA3A expression is modulated during human uterine cervical carcinogenesis. In order to assess whether the Sema3A modulation observed in the 3 mouse models of spontaneous tumorigenesis could be relevant to human tumors, we analyzed by immunohistochemistry SEMA3A expression in tissue biopsy samples of human uterine cervical cancers from patients at different stage of progression (see Methods for the description of the samples). We decided to study human cervical tumors since they represent a prototypic example of multistage carcinogenesis and because of the high similarity and cross-correlation between HPV/E_2 mice and the corresponding human cancer (34). SEMA3A was present in the normal cervix epithelium and in a subset of blood vessels as well. Notably, as observed in HPV/E_2 mice, SEMA3A was highly expressed in the epithelium, in some scattered stroma cells, and in a subset of vessels of CIN-3 lesions, whose progression has been clinically associated with the onset of active angiogenesis (34). In contrast, SEMA3A was barely detectable in cervical SCC, corroborating the data from the mouse models showing of a dramatic downmodulation of this semaphorin in tumors (Figure 3, A and B).

Reexpression of exogenous Sema3A in tumor-bearing RipTag2 mice impairs angiogenesis and tumor growth and increases overall survival. Based on the observed loss of autocrine endothelial Sema3A in the vasculature of late-stage RipTag2 insulinomas, we sought to investigate the effect of reexpressing Sema3A via exogenous *Sema3a* gene delivery on angiogenesis and tumor growth. To this end, we exploited the properties of viral vectors based on the adeno-associated virus (AAV), which allow efficient, safe, and long-lasting therapeutic gene transfer in various tissues and organs (35). In particular, AAV serotype 8 (AAV8) is known to infect both exocrine and endocrine pancreas (36). To achieve specific gene delivery to the pancreas, we established a novel route of administration, entailing the injection of recombinant AAV8 (rAAV8) encoding, under the control of CMV promoter, either LacZ (for control purposes) or Sema3A-Myc (Figure 4A) in the abdominal aorta upon simultaneous clamping of this vessel just below the celiac artery, in order to allow the virus to reach the superior pancreatic-duodenal and lienal arteries and infect pancreas (see Methods). With this procedure, the injection of AAV8 expressing the LacZ gene in RipTag2 and C57BL/6 mice allowed efficient transduction of both exocrine and endocrine pancreas, starting as early as 2 days after injection and persisting for at least 1 month, with an efficiency of 49% of cells infected. LacZ expression was also detectable in the liver and, at very low level, in stomach, kidney, and gut (data not shown). By employing AAV8-Sema3A, we performed in RipTag2 mice a regression trial (RT), i.e., a well-characterized treatment aimed at targeting advanced, well-established cancers and to test the ability of inhibitors to stabilize or regress large tumors and extend life span to a defined end point 4 weeks later (29). We injected 12-week-old tumor-bearing RipTag2 mice with either AAV8-LacZ (control) or AAV8-myc–tagged Sema3A and evaluated the effect of Sema3A on tumor burden and vasculature. Fifty percent of tumor cells were infected by AAV8-Sema3A, an efficiency similar to that obtained with AAV8-LacZ (Supplemental Figure 7A), and Sema3A was highly expressed in its full-length active form (95 kDa), as revealed by Western blot analysis of Sema3A-infected tumors in comparison with control insulinomas (Supplemental Figure 7B). Interestingly, while all untreated RipTag2 mice were hypoglycemic and died around 14 weeks of age, all AAV8-Sema3A–treated mice survived until the end of the trial (16 weeks) and displayed significantly higher blood glucose levels (untreated mice: 21.6 ± 3.4 mg/dl; Sema3A-treated mice: 51.2 ± 5.3 mg/dl; $n = 12$, $P < 0.01$). Evaluating the tumor burden of 14-week-old AAV8-lacZ–treated controls and that of 16-week-old AAV8-Sema3A–treated mice, we noticed a reduction in tumor volume of 65% in treated mice compared with controls (Figure 4B). Hence, based on the finding that tumor volumes at the end (16 weeks) and at the beginning (12 weeks) of the trial were comparable (Figure 4B), it appeared that expression of exogenous Sema3A blocks the growth of RipTag2 insulinomas inducing "stable disease." In addition, as revealed by the Kaplan-Meier survival curve, reexpression of Sema3A in tumors was able to significantly extend the median survival to 8.7 weeks compared with that in controls (Figure 4C).

To assess whether the Sema3A antitumor property was associated with an antiangiogenic effect, we studied the vasculature of treated mice. Interestingly, AAV8-Sema3A significantly reduced tumor blood vessel density (by 41%) (Figure 4, D and G). Even more dramatic effects were observed on the tumor vascular morphology of Sema3A-treated mice compared with controls as revealed by a 3D reconstruction of the vascular network from high-resolution confocal image stacks of vessels stained

with anti–Meca-32 Ab (Figure 4, E and F). This analysis revealed a reduction in vessel branching (53%, Figure 4H) and diameter (46%, Figure 4I) in Sema3A-treated RipTag2 mice compared with untreated animals. Remarkably, AAV8-Sema3A delivery did not affect the normal vasculature of either exocrine pancreas (Figure 4J) or normal islets (data not shown). Therefore, reexpression of Sema3A in late-stage RipTag2 insulinomas results in a selective impairment of cancer angiogenesis, in a significant slowing of tumor growth, and in increased survival.

Sema3A-elicited EC apoptosis and hypoxia precede tumor cell death in RipTag2 insulinomas. Motivated by the clear antitumoral effect exerted by exogenous Sema3A in RipTag2 mice, we sought to investigate the underlying mechanisms. Based on previous reports showing that Sema3A promotes apoptosis (15, 37, 38), we performed a time-course analysis of the apoptotic rate in control and AAV8-Sema3A–treated RipTag2 mice by staining sections with an Ab recognizing the activated form of caspase-3, a well-established apoptotic marker (28). Notably, exogenous Sema3A caused a statistically significant increase in active caspase-3, first in ECs of tumor blood vessels (Figure 5, A and B, arrows) and then in tumor cells (Figure 5, A and C, arrowheads), respectively, 2 and 4 weeks after AAV-mediated gene transfer in the pancreas of 12-week-old RipTag2 mice. Importantly, no apoptotic ECs were detected in blood vessels of normal pancreatic tissue in Sema3A-treated animals (Figure 5D). Since an anti-Ki67 Ab that recognizes dividing cells did not reveal differences in proliferation rates between control and AAV8-Sema3A–treated insulinomas (Figure 5E), we analyzed for the formation of pimonidazole adducts to determine whether Sema3A treatment was interfering with the oxygenation of tumor tissues. Compared with the mild hypoxia noticed in untreated tumors, we observed a transient hypoxic state, likely due to vessel pruning, in 2-week-treated tumors that, however, was no longer present after 4 weeks of therapy (Figure 5F). In contrast, enduring hypoxia has been described in RipTag2 mice during long-term treatment with an antiangiogenic drug targeting the VEGF signaling pathway (39). Moreover, while regrowth was observed in anti–VEGFR-2–treated tumors (5), the 4-week-long AAV8-Sema3A delivery instead caused tumor volume reduction and disease stabilization.

Sema3A increases pericyte coverage of tumor blood vessels in RipTag2 mice and stimulates migration of cultured SMCs. To further investigate the effect of Sema3A on tumor vasculature, we analyzed perivascular cells (pericytes), which are essential blood vessel constituents that support and modulate EC functionality in normal and tumor vasculature (40). A growing body of evidence implicates increased pericyte coverage, together with the reduction in blood vessel density and tortuosity, as a key property of tumor vessel normalization, a process occurring in response to certain antiangiogenic therapies that renders the tumor vasculature more efficient in delivering oxygen and drugs (2, 7). Hence, we analyzed the pericyte coverage of tumor blood vessels after 4 weeks of treatment with AAV8-Sema3A. The expression of molecular markers (41) that define specific subpopulations of pericytes (NG2, α-SMA, desmin, and PDGFR-β) was studied. We observed a substantial increase in pericyte blood vessel coverage (Figure 6A) and content (Supplemental Figure 8, A–C) in AAV8-Sema3A–treated RipTag2 mice compared with controls. Quantitation of pericyte markers localized in close proximity to EC-lined blood vessels revealed increased pericyte coverage (by 44% for $NG2^+$ cells, 45% for α-SMA^+ cells, and 40% for PDGFR-β^+ cells) in Sema3A-treated versus control tumors (Figure 6, B–D). A similar increase in pericyte coverage was detected with desmin staining (data not shown).

In the 2-week-long Sema3A treatment trial, in which we detected increased EC apoptosis (Figure 5, A and B), we also observed less-pronounced pericyte coverage, similar to that of untreated tumors (Supplemental Figure 8D). The fact that most of the Sema3A-treated apoptotic vessels lacked mural cells suggested that pericyte coverage could somehow exert a protective role against Sema3A-elicited EC apoptosis (Supplemental Figure 8E). These findings are consistent with data showing that VEGF blockade prunes nascent vessels that are not covered by pericytes (2, 42). We infer that the noncoated vessels undergoing apoptosis gradually disappear, such that by 4 weeks the pericyte-covered vessels become predominant. Recently it has been shown that loss of the G protein signaling 5 gene (*Rgs5*) results in pericyte maturation, vascular normalization, and, as a consequence, marked reduction in tumor hypoxia and blood vessel leakiness (43). By real-time RT-PCR, we observed that *Rgs5* and *NG2* transcripts were strongly downregulated and upregulated, respectively, in AAV8-Sema3A–treated tumors compared with controls (Figure 6E), suggesting increased pericyte maturation in treated tumors.

Of note, while we did not detect significant Sema3A expression in pericytes (data not shown), in these cells the expression pattern of Nrp1, Nrp2, PlxnA1, and PlxnA2 was similar to that observed in ECs during tumor progression in RipTag2 mice (Supplemental Figure 6). These observations together with the fact that human aortic SMCs also express Nrp1 (44) (Supplemental Figure 9G) suggested that Sema3A might act as a chemoattractant for these cells or their precursors. Consistent with this possibility, we found that recombinant Sema3A, while inhibiting EC motility, elicited SMC migration in chemotaxis assays (Figure 6F and Supplemental Figure 9, A and B). In contrast, Sema3A did not significantly affect SMC proliferation or apoptotic rate (Supplemental Figure 9, C–F). Therefore, Sema3A can also favor vascular coverage by mobilizing pericytes and mediating their association with remodeling blood vessels. Taken together, our observations indicate that Sema3A reexpression in tumors inhibits angiogenesis and cancer growth, along with the normalization of remaining blood vessels.

Sema3A inhibits β_1 integrin activation in tumor ECs but not in pericytes. Integrin adhesive receptors are crucial regulators of cancer angiogenesis and metastasis (45), and preclinical studies implicated some integrin heterodimers, such as $\alpha_v\beta_3$ and $\alpha_5\beta_1$, as potential targets for antiangiogenic therapy (46). Integrins undergo conformational modifications that regulate their affinity for ECM ligands, and the Sema/Nrp/Plexin signaling pathways have been shown to inhibit integrin function in ECs and several other cell types (17, 46). Thus, we hypothesized that regulation of integrin activation in vascular ECs and pericytes could be a major signaling mechanism by which Sema3A overexpression in tumors could inhibit neoangiogenesis and promote pericyte coverage of remaining blood vessels.

To address this possibility, we first profiled by real-time RT-PCR the expression in the RipTag2 model of integrins previously implicated in tumor angiogenesis (46). Consistent with previous data (47), we detected a significant increase in *Itga5* and *Itgb1* mRNA in angiogenic islets and tumors compared with normal islets; both *Itgav* and *Itgb3* genes were also more actively transcribed, albeit at lower levels (Figure 7A). In a consistent manner, the expression of total (i.e., active and inactive) α_5 and β_1 integrin subunits in vas-

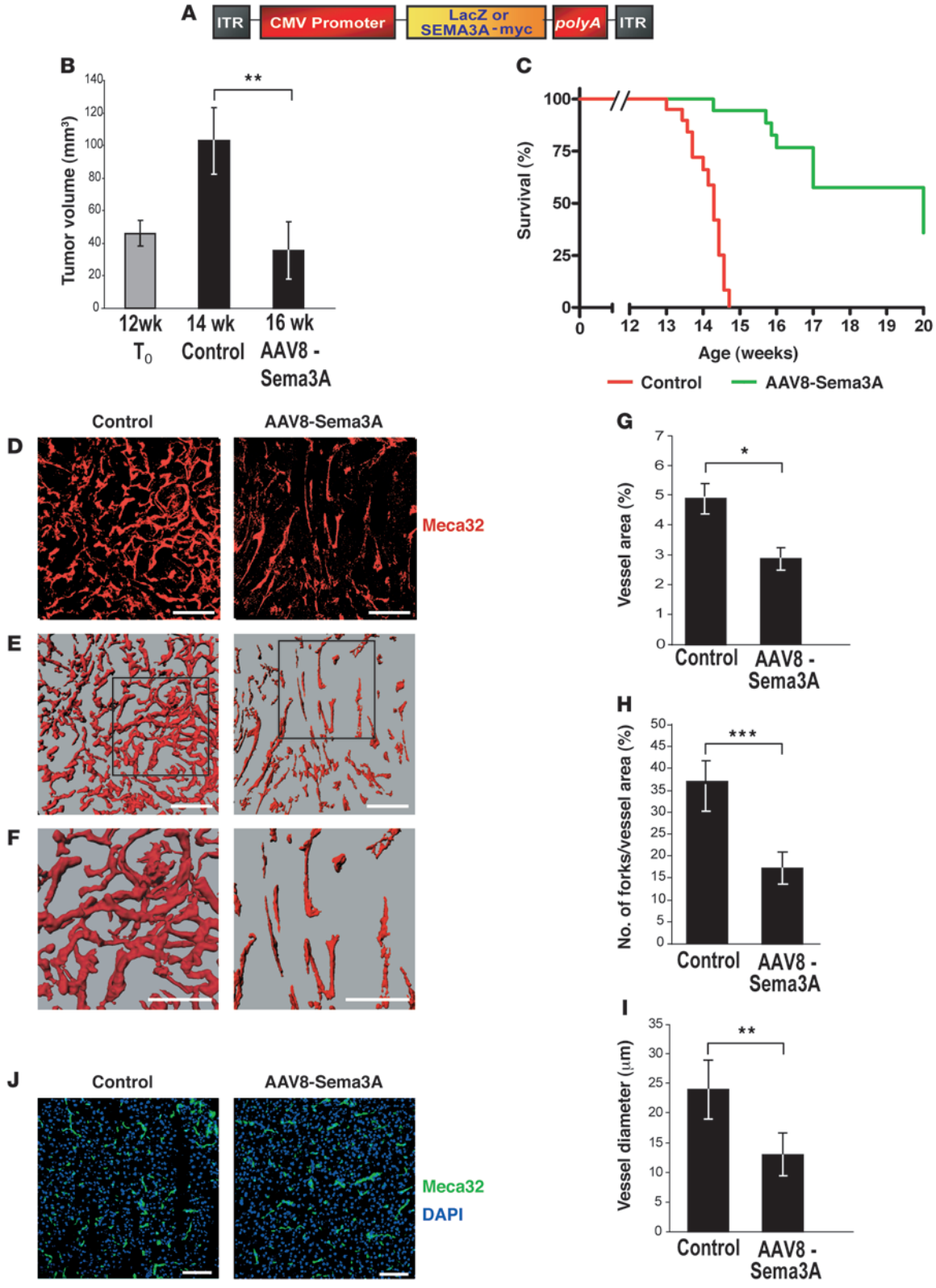
A
ITR
CMV Promoter
LacZ or SEMA3A-myc
polyA
ITR
B
Tumor volume (mm3)
**
12wk T0
14 wk Control
16 wk AAV8 - Sema3A
C
Survival (%)
Age (weeks)
Control
AAV8-Sema3A
D
Control
AAV8-Sema3A
Meca32
E
F
G
Vessel area (%)
*
Control
AAV8 - Sema3A
H
No. of forks/vessel area (%)
***
Control
AAV8 - Sema3A
I
Vessel diameter (μm)
**
Control
AAV8 - Sema3A
J
Control
AAV8-Sema3A
Meca32
DAPI

Figure 4
Restoring Sema3A expression in RipTag2 tumors inhibits angiogenesis and blocks tumor growth. (**A**) rAAV8 vector expresses myc-tagged Sema3A or LacZ under the control of the constitutive CMV promoter. (**B**) Tumor volume of AAV8-Sema3A–treated mice was reduced by 65% compared with that of controls (n = 10 and n = 12 for 12-week and 14-week RipTag2 controls, respectively; n = 12 for AAV8-Sema3A–treated 16-week-old mice; $^{**}P < 0.001$). (**C**) Kaplan-Meier survival curve generated by injecting 12-week-old RipTag2 mice with either AAV8-Sema3A (n = 20) or AAV8-lacZ (n = 20) and monitoring their survival; Sema3A reexpression in tumors significantly extended median survival to 8.7 weeks compared with controls (log-rank [Mantel-Cox] test, $P < 0.0001$). Values are mean ± SD. (**D** and **G**) Vessel density, as assessed by Meca-32 immunostaining, was significantly reduced in AAV8-Sema3A tumors compared with controls (41% reduction in vessel area, $^{*}P < 0.01$). (**E**) High-resolution confocal image stacks of vessels stained with anti–Meca-32 Ab were reconstructed by isosurface rendering using Imaris software. Tumor vascular morphology of Sema3A-treated mice was more linear, less branched, and with a smaller diameter compared with controls. (**F**) Higher magnification of the boxed areas in **E** of the 3D reconstruction in treated and untreated tumors. Analysis of confocal images revealed a reduction in vessel branching (53%, $^{***}P < 0.0001$) (**H**) and vessel diameter (46%, $^{**}P < 0.001$) (**I**). Results are mean ± SD of 5 fields per mouse from a total of 10 mice per treatment group. (**J**) AAV8-Sema3A treatment did not affect normal vessels of exocrine pancreas. Scale bars: 50 μm.

cular ECs of angiogenic and tumor islets was 67% and 69% higher than in normal islets, respectively (Figure 7, B and D, and data not shown), confirming previous studies performed in the same mouse model by using an anti-α_5 Ab (47).

Next, to directly investigate possible regulation in vivo by Sema3A of these integrins, we took advantage of the conformation-sensitive rat monoclonal Ab 9EG7, which recognizes the active form of mouse β_1 integrins (48, 49). Even though total β_1 integrin subunit was expressed at similar levels in blood vessels of angiogenic islets and tumors (Figure 7, B and D), the amount of active β_1 in tumor ECs was 51% higher than in ECs of angiogenic islets (Figure 7, C and D). Of note, increased β_1 integrin activation in tumor versus angiogenic islets inversely correlated with endogenous levels of Sema3A (Figure 1A and Figure 2A). Importantly, while the amount of total β_1 integrins did not change in tumor endothelium in response to the *Sema3a* gene therapy (Figure 7F), we observed that active β_1 integrins were 53% lower in ECs of Sema3A-treated RipTag2 tumors than in ECs of control insulinomas (Figure 7, E and G). Disruption of integrin-mediated EC attachment to ECM results in activation of programmed cell death by a process termed anoikis (50). Thus, inhibition of integrin function by exogenous Sema3A could represent a major mechanism in the induction of tumor EC apoptosis we noticed in treated RipTag2 mice.

It has been recently shown that β_1 integrin is essential for mural cell adhesion and blood vessel wall stability (51). Since Sema3A inhibited β_1 integrin activation and elicited tumor EC apoptosis, we sought therefore to evaluate whether AAV8-Sema3A also modulated β_1 integrin function in the tumor pericytes that plentifully covered blood vessels upon treatment. Similar to what was observed in vascular ECs, total and active β_1 integrin levels were greater in pericytes of angiogenic and tumor islets than in their normal counterparts (Supplemental Figure 10, A and B). Consistent with the observed promigratory effects exerted by Sema3A on SMCs (Figure 6F), we observed no statistically significant inhibition of mural β_1 integrin activation between control and Sema3A-treated RipTag2 mice (Supplemental Figure 10, C and D). Taken together, these results indicate that reexpression of exogenous Sema3A in tumors exerts differential effects on ECs and pericytes.

Endogenous Sema3A controls the onset of angiogenesis during tumor progression. To directly test whether Sema3A is an endogenous angiogenesis inhibitor able to counterbalance angiogenic factors (such as VEGF-A) during the angiogenic switch, we sought to impair its function and assess whether this could influence angiogenesis and tumor progression. To this aim, we employed an effective and highly selective Sema3A pharmacological inhibitor, SM-216289, that was previously shown to enhance in vivo axon regeneration and angiogenesis at the site of spinal cord injury (13, 52).

First, we performed an in vitro assay aimed at testing the angiogenic potential of islets purified from RipTag2 mice (53, 54). We embedded in a collagen gel ECs and RipTag2 angiogenic islets in the presence or absence of the SM-216289 inhibitor or of an anti-VEGF Ab. Compared with the untreated controls (Figure 8C), SM-216289 dramatically increased EC radial migration and assembly into capillary-like structures directed toward the angiogenic islets (Figure 8D). In contrast, as previously described (54), a neutralizing anti-VEGF Ab severely attenuated the angiogenic response (Figure 8E). Notably, addition of the Sema3A inhibitor rescued the angiogenic potential of islets simultaneously incubated with the VEGF-blocking Ab (Figure 8F). To further verify the selectivity of SM-216289, we tested its effect on the inhibition of EC migration by Sema3A, Sema3E, and Sema3F. In accordance with previously reported neuron growth cone collapse assays (13), SM-216289 impaired Sema3A but neither Sema3E nor Sema3F inhibitory activity on EC migration (Figure 8G).

Next, to assess whether the inhibitory activity of endogenous Sema3A was critical to regulating in vivo the onset of angiogenesis and tumor growth, by means of osmotic minipumps we delivered to the pancreas of RipTag2 mice either SM-216289 or saline buffer. We implanted minipumps at 8.5 weeks of age and continuously administered SM-216289 for 2 weeks (see Methods). Indeed, in this time window we observed that in RipTag2 mice, Sema3A expression increased concomitantly with the angiogenic switch. Moreover, at 10.5 weeks of age, RipTag2 mice display activated angiogenesis, a very low percentage of tumor incidence, and low tumor burden (29). Notably, continuous local administration of SM-216289 to the pancreas of RipTag2 mice dramatically increased tumor incidence (by 50%) and tumor volume (by 84%) compared with controls (Figure 8, H–J). Moreover, almost 50% of SM-216289–treated mice displayed increased tumor number as compared with controls that showed an average of 1 tumor per mouse (data not shown). Finally, we evaluated the effect of Sema3A inhibition on tumor angiogenesis and observed that 2 weeks of SM-216289 treatment enhanced angiogenesis by 36% compared with saline-treated controls (Figure 8K). Importantly, SM-216289 did not promote tumors directly, as revealed by proliferation assays on βTC3 cells, derived from RipTag2 tumors (5) and other murine and human cancer cell lines (Supplemental Figure 11) that did not express significant levels of Sema3A (data not shown).

Finally, to further confirm the inhibitory effect of Sema3A on angiogenesis during tumor progression, we performed a prevention trial (PT), originally designed to assess the effects of a compound in preventing the initial angiogenic switching and therefore preventing tumor formation (29, 41). The PT started by injection of

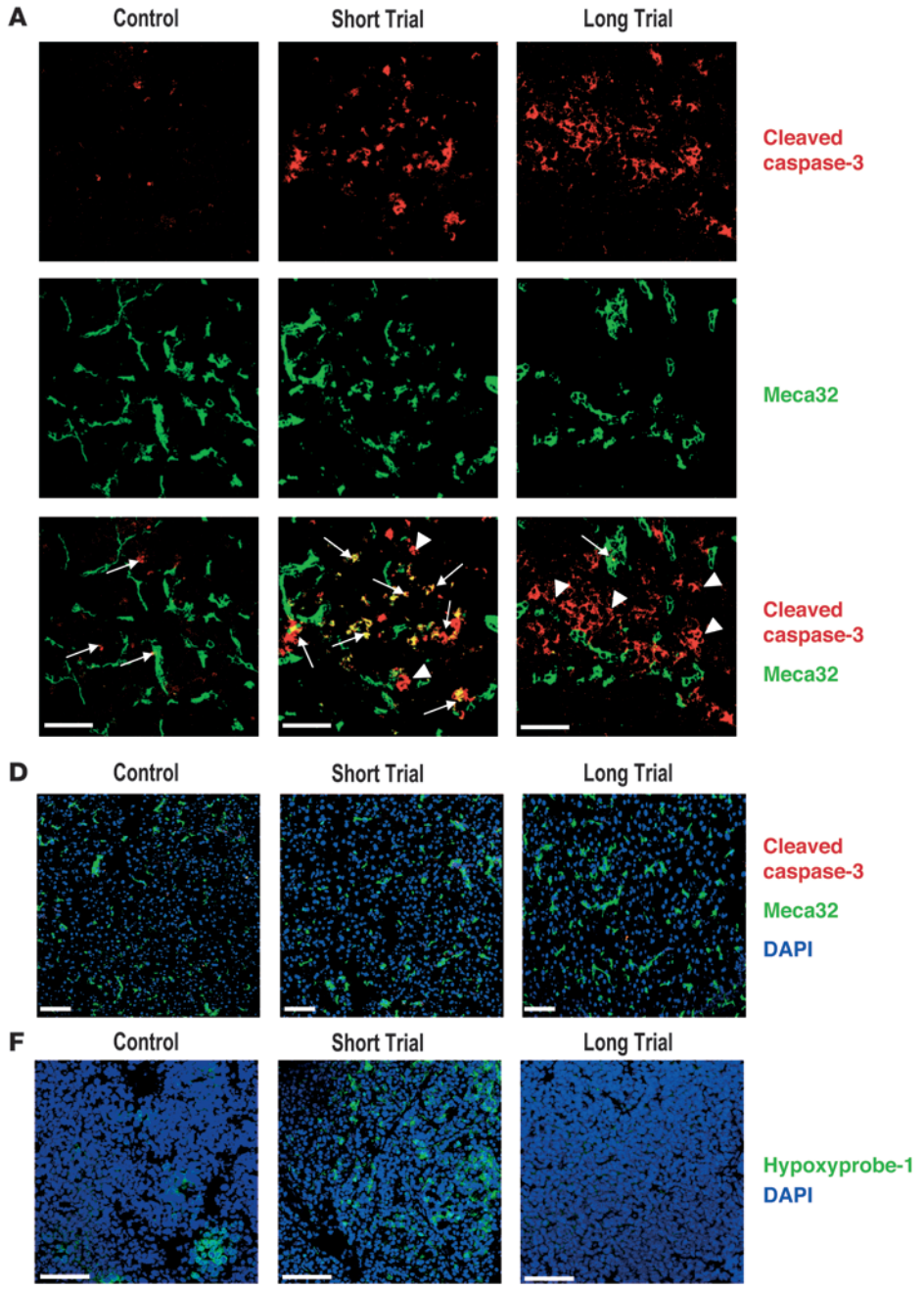

Figure 5

Sema3A induces apoptosis first in vascular ECs and then in tumor cells. (**A**) Compared with 14-week-old AAV8-LacZ controls, AAV8-Sema3A treatment of 12-week-old RipTag2 mice promoted apoptosis in ECs (arrows) and tumor cells (arrowheads) 2 (short trial) and 4 (long trial) weeks after AAV gene delivery, respectively. EC apoptotic rate was detected by colocalization of Meca-32 (green) with activated caspase-3 (red). Images are representative of 5 fields per mouse from a total of 10 mice per 2- and 4-week-long treatment. (**B** and **C**) Percentage of cleaved caspase-3+ cells on total cells in the short (**B**) and long (**C**) trial, compared with controls (**$P < 0.001$). (**D**) Upon Sema3A treatment, no apoptotic ECs were detected in blood vessels of normal pancreatic tissue in either short or long trial. (**E**) In long trials, anti-Ki67 immunostaining revealed no difference in proliferation rate in AAV8-Sema3A–treated compared with control animals. (**F**) Islet tumor hypoxia as detected by the formation of pimonidazole adducts (green). In short trials, Sema3A transiently enhanced tumor hypoxia compared with control, while in long trials, Sema3A-treated insulinomas were normoxic. Values are mean ± SD (n = 10 mice per 2- and 4 week-long treatment). Scale bars: 50 μm.

AAV8-Sema3A in RipTag2 pancreas at 5 weeks, when mice harbor hyperplastic/dysplastic islets, and ended at 10.5 weeks, when the first small tumors began to appear. Interestingly, compared with controls, we observed in 10.5-week-old Sema3A-treated mice a 60% reduction in the number of angiogenic islets (Figure 8L). Moreover, while small insulinomas appeared in 25% of control RipTag2 mice (data not shown), treatment with Sema3A completely prevented tumor development. Thus, early Sema3A overexpression during

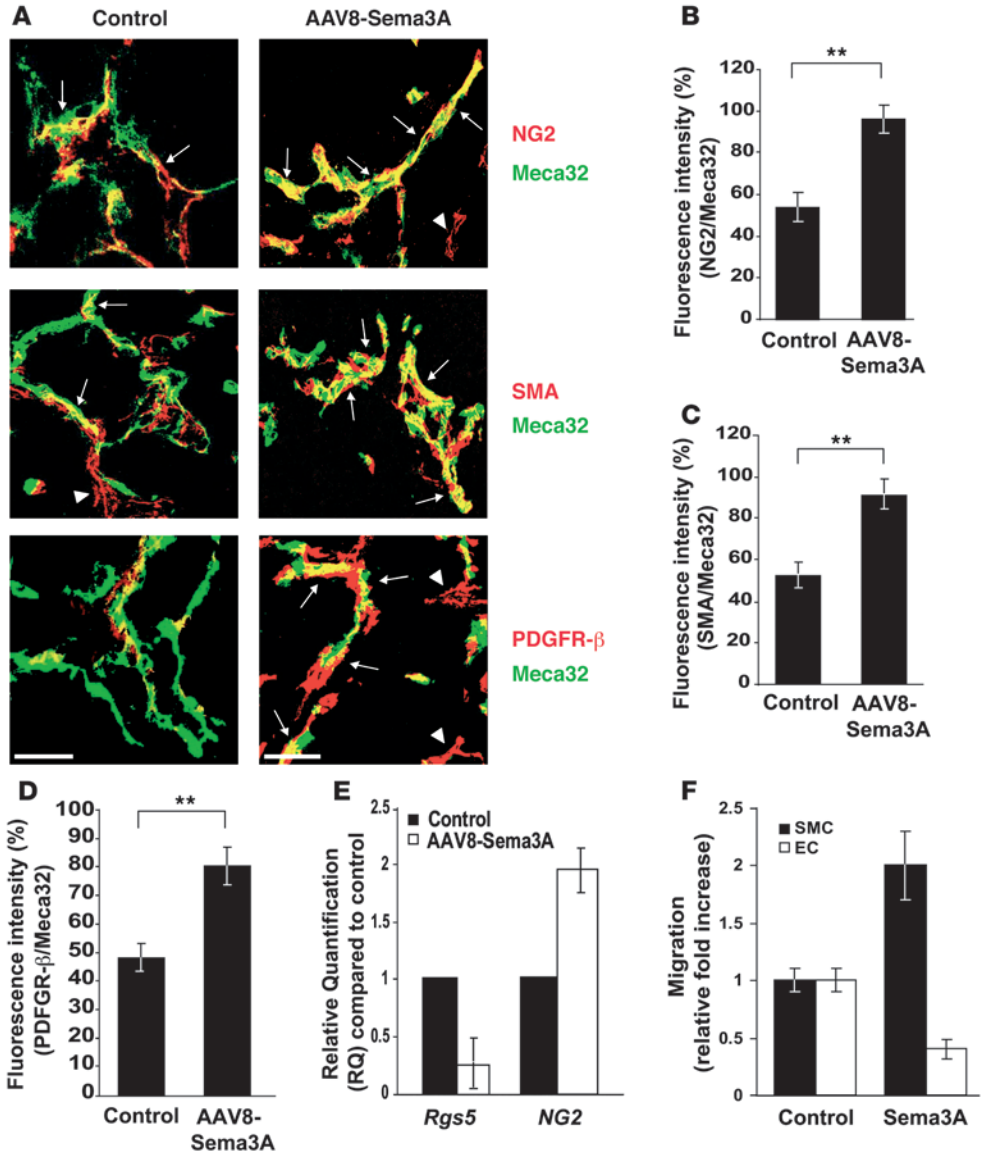

Figure 6
Sema3A induces pericyte coverage of tumor blood vessel and promotes SMC migration. (**A**) Fluorescence confocal microscopy brought to light an increase in pericyte coverage of tumor blood vessels after 4 weeks of AVV8-Sema3A treatment compared with controls. Pericyte coverage was evaluated by analysis of colocalization (arrows) of Meca-32 with NG2, α-SMA, or PDGFR-β. Arrowheads indicate pericytes in the immediate vicinity of ECs. Images are representative of 5 fields per mouse from a total of 10 mice per treatment group. Scale bars: 50 μm. (**B**–**D**) Percentage of colocalization of pericyte markers on tumor ECs; quantification analysis revealed an increase in pericyte coverage of 44% for NG2$^+$ cells (**B**), 45% for SMA$^+$ cells (**C**), and 40% for PDGFR-β$^+$ cells (**D**) in AAV8-Sema3A–treated versus untreated tumors (**$P < 0.001$). Values are mean ± SD ($n = 10$ animals per treatment group). Pericyte colocalization was measured as fluorescence intensity ratio between red (NG2, SMA, and PDGFR-β) and green (Meca-32) channels (see Methods). (**E**) While the *NG2* gene was upregulated, the *Rgs5* gene, a marker of activated pericytes, was strongly downregulated in AAV8-Sema3A–treated tumors (4 weeks) compared with controls, as detected by real-time RT-PCR. (**F**) Human recombinant Sema3A inhibited EC motility and enhanced human SMC migration in chemotaxis assays. Relative cell migration is expressed as fold increase compared with control unstimulated cells. Values are mean ± SD of 4 independent experiments.

tumor progression delays the angiogenic switch and does not allow tumor formation. Taken together, these data support the concept that Sema3A is an effective endogenous angiogenesis inhibitor that counteracts proangiogenic factors (such as VEGF-A) to regulate the onset of the angiogenic process in premalignant lesions. Endothelial Sema3A disappears at later stages of tumor progression, favoring excessive but abnormal vessel formation and tumor growth.

Discussion

A growing body of evidences implicates Sema3A and Sema3F as antiangiogenic and tumor-suppressing agents (12, 14, 16, 21, 55). However, the roles played by Sema3s during the distinctive lesional stages that characterize the natural history of multistep tumor progression are essentially unknown (30, 56). Herein, studying 3 different genetically engineered mouse models of

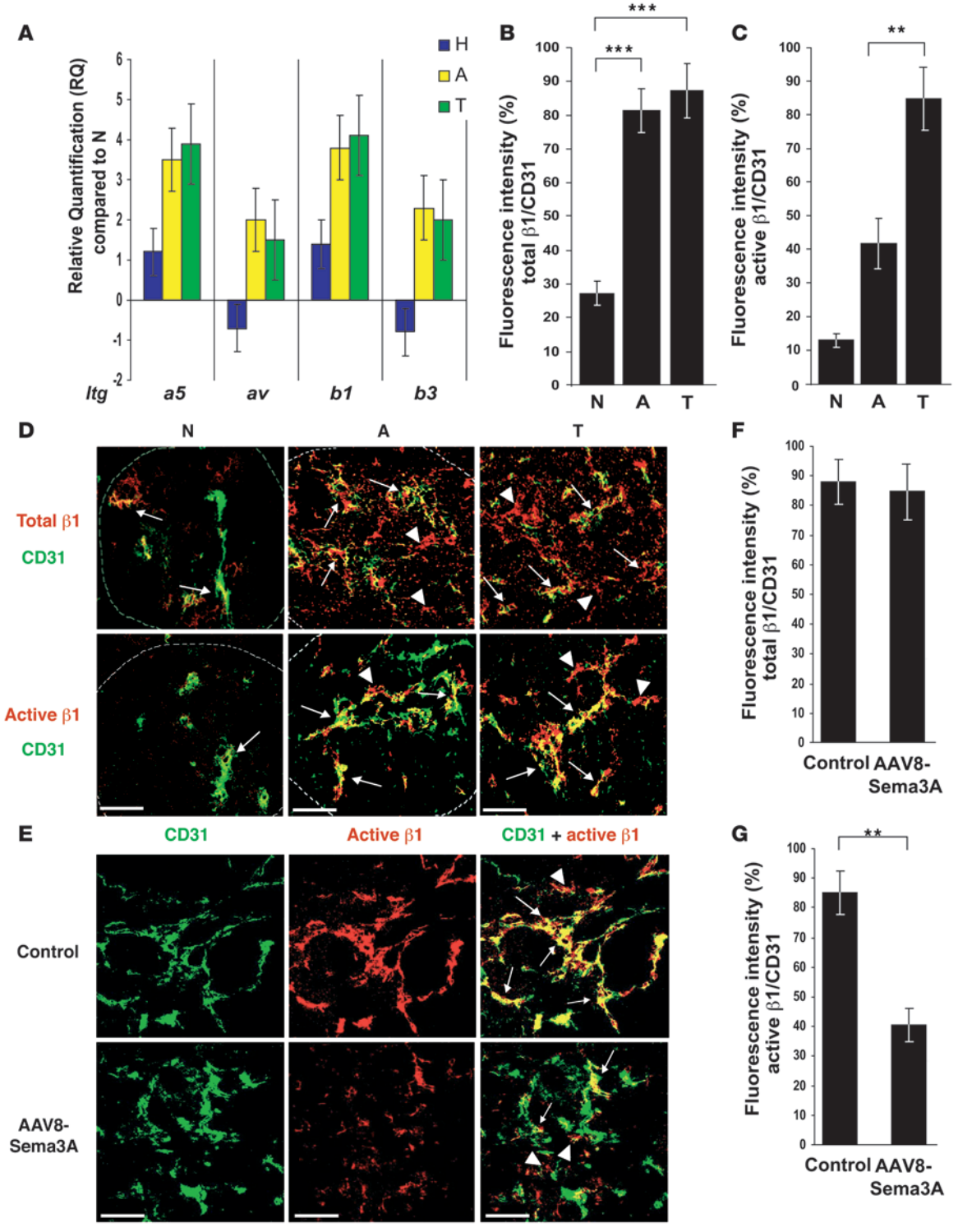
A
Relative Quantification (RQ) compared to N
H
A
T
ltg
a5
av
b1
b3
B
Fluorescence intensity (%) total β1/CD31
***
***
N
A
T
C
Fluorescence intensity (%) active β1/CD31
**
N
A
T
D
N
A
T
Total β1
CD31
Active β1
CD31
E
CD31
Active β1
CD31 + active β1
Control
AAV8-Sema3A
F
Fluorescence intensity (%) total β1/CD31
Control
AAV8-Sema3A
G
Fluorescence intensity (%) active β1/CD31
**
Control
AAV8-Sema3A

Figure 7
Sema3A inhibits β_1 integrin activation in tumor ECs. (**A**) Real-time RT-PCR analysis of integrin expression during RipTag2 tumorigenesis showed an increase in *Itga5* and *Itgb1* mRNA in both angiogenic islets and tumors, compared with normal islets. RQ values are mean ± SD of 4 experiments. Total RNA derived from a pool of islets of 10 mice per stage. (**B** and **D**) Confocal analysis revealed an increase in total β_1 integrins in ECs of angiogenic islets and tumors, compared with normal islets, as detected by colocalization of CD31 (green) with total β_1 (red) (**D**); graph shows the percentage of total β_1 integrin colocalized with ECs (**B**) (67% increase in angiogenic islets, 69% increase in tumors vs. normal islets, $^{***}P < 0.0001$). (**C** and **D**) Colocalization of CD31 (green) with active β_1 integrins (red) showed an increase in β_1 integrin activation in tumors compared with angiogenic islets and normal islets (**D**); graph shows the percentage of active β_1 integrin present on ECs (**C**) (51% increase in tumors vs. angiogenic islets, $^{**}P < 0.001$). (**E**) Four-week-long AAV8-Sema3A treatment induced a decrease in active β_1 integrins (red) in tumor CD31-positive (green) ECs compared with controls. (**F** and **G**) Percentage of total and active β_1 integrins present on tumor ECs. β_1 integrin activation decreased by 53% in AAV8-Sema3A–treated mice compared with controls (**G**, $^{**}P < 0.001$). Arrows and arrowheads, respectively, indicate total and active β_1 integrin colocalization with ECs and pericytes. Values are mean ± SD ($n = 10$ animals per group). Dotted lines indicate normal islets and lesions surrounded by the exocrine pancreas. Scale bars: 50 μm.

multistage tumorigenesis, we unveil the existence of endothelial Sema3A autocrine loops in premalignant lesions that are lost in overt cancer. These data strengthen the hypothesis that Sema3A autocrine loops, while involved in physiological angiogenesis (10, 19), need to be downregulated to allow tumor progression (14). Interestingly, the modulation of Sema3A expression we observed in ECs of RipTag2 angiogenic and tumor islets is in line with the stage-specific molecular changes that occur in blood vessels during multistep carcinogenesis and represent distinguishing features for dysplastic versus tumor vasculature in both RipTag2 and HPV/E_2 mice (57, 58), as well as in the Alb-Tag mouse model of hepatocellular carcinogenesis (59).

In agreement with its well-characterized antitumoral and antiangiogenic effect (60), Sema3F was modulated similarly to Sema3A in all 3 mouse models, further suggesting that Sema3F can act as a regulator of tumor angiogenesis. However, in all 3 models and in contrast to Sema3A, Sema3F was mainly expressed by the dysplastic epithelium, while the Sema3F coreceptor Nrp2 was expressed in both dysplastic and tumor vessels, suggesting the existence of a paracrine inhibitory Sema3F/Nrp2 pathway between tumor cells and ECs, as also recently proposed by others (61). Moreover, Sema3F, while being expressed in human melanoma, bladder, and prostate tumors, is lost during tumors metastasis (55). Based on our observations, we hypothesize that a similar Sema3F/Nrp2 suppressive pathway can be lost during tumor progression. We therefore predict that Sema3A and Sema3F could exert a synergistic inhibitory effect on tumor angiogenesis and growth in RipTag2 mice. Future investigations comparing simultaneous and combined delivery of both Sema3A and Sema3F in tumors will help clarify these aspects.

We established a new method for somatic gene transfer involving AAV8 that enabled pancreatic targeting and thereby restoration of Sema3A expression in late-stage RipTag2 insulinomas. In short RTs of 2 weeks, exogenous Sema3A elicited programmed cell death in the islet tumors, mainly in ECs. Accordingly, after 4 weeks of elevated expression of Sema3A consequent to the AAV8-mediated gene therapy, we noticed a significant reduction in vessels density and branching, associated with induction of tumor cell apoptosis, shrinkage in tumor volume, and increased pericyte coverage. Our observations support the concept that Sema3A reexpression produces dual effects, of vessel pruning early on following reexpression and increased pericyte coverage later on, with the final effect of, respectively, reducing tumor growth and giving rise to normalized and ostensibly more functional blood vessels.

It is conceivable that loss of angiogenesis inhibition by endogenous Sema3A is important for accelerating the initial angiogenic switch that occurs in the pre-malignant phase of tumor development. At this time, Sema3A may counterbalance the stimulatory effects of angiogenic growth factors (AGFs), such as VEGF-A and bFGF (24), thus allowing for a regulated neovascularization. In the later stages of progression, cancer cells could induce a greater unbalance between AGFs and Sema3A in favor of the former, for example, by eliciting *Sema3a* promoter methylation and silencing, as shown for other genes (62). The ensuing increase in the AGF/Sema3A ratio could in turn elicit the formation of a more abundant and extensively branched, but less functional and chaotic vasculature. To better characterize the role of endogenous Sema3A during the early phases of RipTag2 tumorigenesis, we either impaired or increased its activity by delivering to premalignant pancreatic tumors the Sema3A inhibitor SM-216289 or an AAV-8 virus carrying the *Sema3a* gene, respectively. Our observations that inhibition of endothelial Sema3A by SM-216289 at the initial stages of insulinoma development dramatically increases the number of angiogenic islets as well as tumor incidence and growth, while the delivery of exogenous Sema3A exerts the opposite effect, provide compelling evidence that in RipTag2 mice, endogenous Sema3A restrains the onset and the rate of angiogenesis, likely by counteracting the activity of AGFs.

The effects on the cancer vasculature, which we noticed after therapeutic restoration of Sema3A by somatic gene transfer, recall the notion of vascular normalization proposed by Jain and colleagues, whereby antiangiogenic drugs prune, remodel, and increase pericyte coverage of otherwise abnormal tumor vessels, which therefore become more efficient in blood flow and consequently in delivering cytotoxic drugs and oxygen for radiotherapy (2, 4). Usually, the tumor vessel normalization that occurs after antiangiogenic therapy gives rise to a 5- to 6-day-long normalization window, during which association with radiation or chemotherapy leads up to a better therapeutic outcome (2, 7). Our data suggest that Sema3A could further extend such a normalization window, hence providing an ampler time for combination with other anticancer therapies.

Over the past 5 years, the clinical development of antiangiogenic agents has grown remarkably; currently there are 3 inhibitors of VEGF-A pathway approved for use in cancer therapy (63) and more than 50 in various stages of preclinical and clinical evaluation. Among the former is bevacizumab, a VEGF-A–specific Ab recently FDA approved for use with standard chemotherapy as first and second line of treatment in several metastatic solid tumors (63). Despite bevacizumab's increased response rates against metastatic colorectal, lung, and breast cancers, its survival benefit when associated with first-line chemotherapy was progressively lost due to acquisition of resistance to the antiangiogenic therapy in metastatic colorectal and breast cancers (4). Similarly,

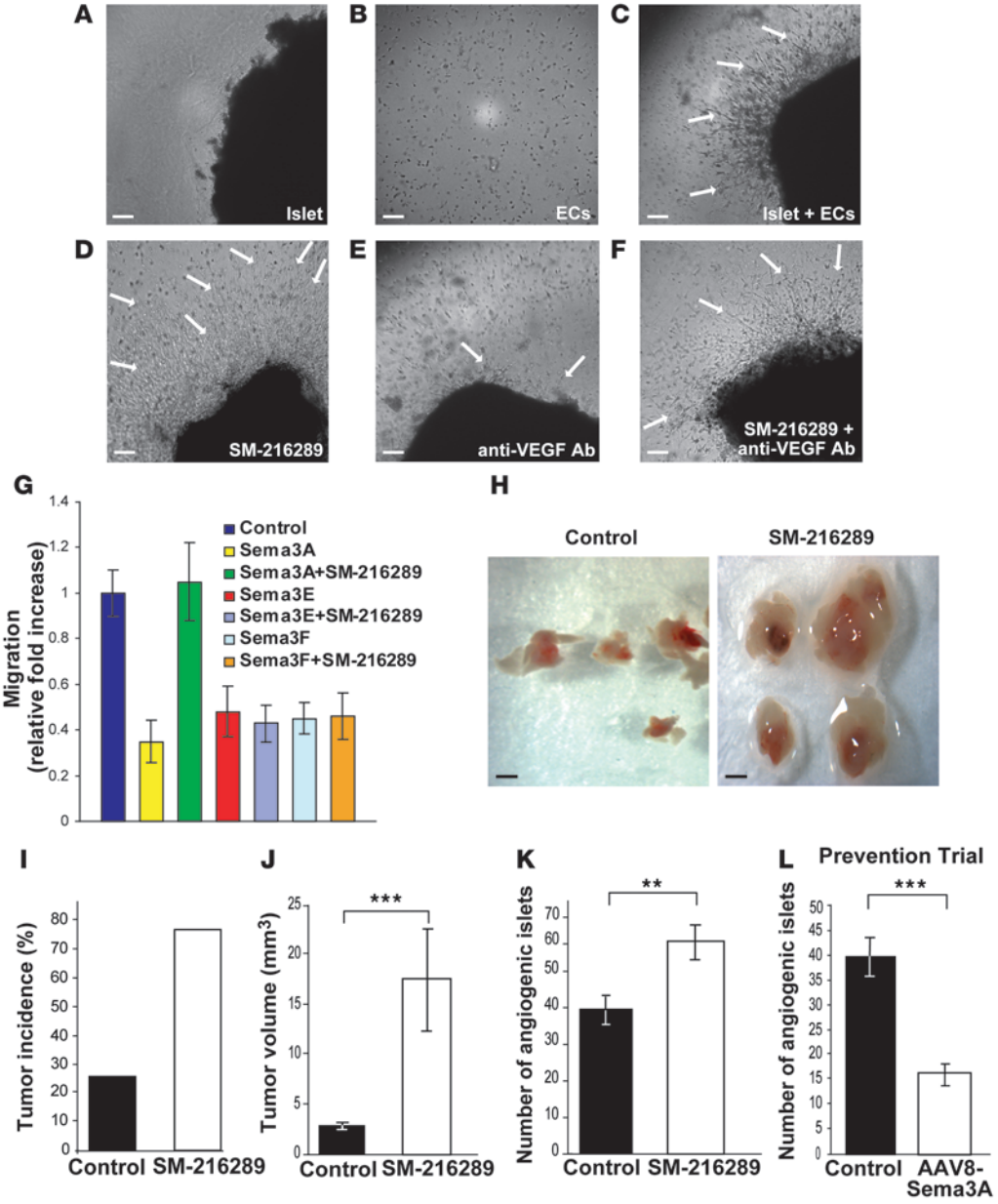

Figure 8

Endogenous Sema3A regulates the angiogenic switch during tumor progression. Sema3A inhibition increased the angiogenic activity of islet purified from 10.5-week-old RipTag2 mice in a collagen gel bioassay. (**A**) Angiogenic islets in the absence of ECs and (**B**) ECs without islets in a collagen gel. (**C**) Angiogenic islets in the absence (untreated control) (**D**) or presence of SM-216289 alone (**E**) or VEGF-blocking Ab alone (**F**) or both SM-216289 and VEGF-blocking Ab, were embedded into a 3D collagen matrix containing ECs. SM-216289 neutralized the inhibitory effect induced by an anti-VEGF Ab (arrows). Scale bars: 50 μm (**A**–**F**). (**G**) EC migration in the absence or presence of SM-216289 and Sema3A, Sema3E, or Sema3F. SM-216289 did not interfere with either Sema3E or Sema3F inhibitory activity. (**H**) SM-216289 or saline were locally administrated by osmotic minipumps in 8.5-week-old RipTag2 mice for 2 weeks. Gross pathology images of pancreatic islets and tumors from 10.5-week-old animals after 2 weeks of saline treatment showing angiogenic islets and small tumors (left panel) compared with a significantly enhanced tumor volume due to continuous inhibition of Sema3A (right panel). Scale bars: 800 μm (**H**). (**I**) Increased tumor incidence in SM-216289– versus saline-treated animals (by 50%). (**J**) Increased tumor volume in SM-216289–treated animals compared with controls (84%, $^{***}P < 0.0001$). (**K**) SM-216289 treatment enhanced the number of angiogenic islets compared with controls (36%, $^{**}P < 0.001$). (**L**) In a PT, Sema3A overexpression delayed the angiogenic switch, as indicated by a 60% reduction in the number of angiogenic islets in AAV8-Sema3A–treated mice compared with controls ($n = 12$, $^{***}P < 0.0001$).

preclinical RTs in RipTag2 mice showed that VEGFR-2 blockade only transiently inhibits tumor growth (5). More recently, it has been reported that, in tumor xenograft models resistant to VEGF(R) inhibitors, a neutralizing monoclonal Ab against PlGF can impair tumor angiogenesis, growth, and metastasis (6). However, such an anti-PlGF Ab did not inhibit the growth of pancreatic islet tumors of transgenic RipTag2 mice (64). In contrast to anti–VEGFR-2 and anti-PlGF, by employing Sema3A as a single

agent, we were able to impair tumor angiogenesis and growth, producing stable disease and significantly extending the life span of RipTag2 mice, as revealed by the Kaplan-Meier survival curve. It is worth noting that, in contrast to what was described in long-term anti-VEGF therapies (39), we did not observed long-lasting tumor hypoxia after Sema3A treatment, suggesting that the increased tumor oxygenation could be responsible for the observed cancer stabilization and increased survival. Moreover, Sema3A treatment did not damage the vasculature of exocrine pancreas and normal islets (or other tissues of the animal), indicating that its activity is limited to blood vessels undergoing active remodeling, making this molecule attractive for potential future translation into the clinic. We conclude that while on one hand, the levels of Sema3A proportionally restrain the amount of blood vessels and hence the amount of tumor cells that can be fed, on the other hand, Sema3A promotes the maturation of the surviving vasculature and does not trigger the apoptosis of ECs within preexisting pericyte-covered mature blood vessels. Our observation that most of the apoptotic vessels in Sema3A-treated versus untreated tumors lack pericytes supports the concept that mural cell coverage exerts a protective role against Sema3A-elicited EC apoptosis. This dual regulation of EC apoptosis by Sema3A translates into a long-lasting stabilization of small-size insulinomas that coexists with blood vessel normalization and normoxia upon AAV8-mediated delivery of Sema3A in RTs.

Recently, it has been shown in tumor xenograft models that Nrp1 blockade was able to decrease angiogenesis and synergize with an anti-VEGF Ab (65). Our data suggest that to appropriately apply new antiangiogenic therapies based on Nrp1 inhibition to different cancer histotypes, the expression levels of Sema3A should be first carefully analyzed, in order to avoid potential opposite effects, such as enhanced tumor angiogenesis and growth, due to the inhibition of Sema3A antiangiogenic signaling. These preventive analyses could help to valorize and to favor drugs that selectively block the VEGF-A binding site of Nrp1 without affecting Sema3A signaling in tumors, such as some recently developed Abs raised against the b1-b2 domains of Nrp1 (65).

We (10) and others (17) have previously shown that Sema3s regulate integrin activation and function in ECs and other cell types. While determining the mechanisms of Sema3A activity, we found that during tumor progression, β_1 integrin activation increases in both ECs and pericytes. Moreover, we showed for the first time to our knowledge an in vivo inhibitory effect of Sema3A on endothelial β_1 integrins associated with an impairment of tumor angiogenesis and growth. $\alpha_5\beta_1$ integrin is highly expressed in tumor vasculature in RipTag2 mice, and inhibition of β_1 integrin activation in tumor ECs is in line with previous data showing that selective $\alpha_5\beta_1$ integrin antagonists inhibit tumor angiogenesis and growth in preclinical models (66). Interestingly, it has been reported that inhibition of $\alpha_5\beta_1$ integrin signaling induces caspase-3– and caspase-8–dependent EC apoptosis in experimental angiogenesis (67), suggesting that the tumor EC apoptosis we observed after AAV8-Sema3A treatment is likely due to the impairment of $\alpha_5\beta_1$ integrin activation. Interestingly, we did not detect any reduction in β_1 integrin activation in pericytes, implying that Sema3A may have different effects on tumor ECs and pericytes. Our observations that Sema3A promotes migration of cultured SMCs and leads to an increased pericyte content in RipTag2 insulinomas further support the notion that while Sema3A behaves as an inhibitor for tumor ECs, it could display attractive effects on pericytes or their progenitors, which can differentiate in mature pericytes and lead to vascular stabilization (68). How could Sema3A behave as a chemoattractant for pericytes? An attractive hypothesis could be represented by the synergism between Sema3A and the NO/soluble guanylate cyclase (sGC)/cGMP pathway in pericytes. Indeed, it has been previously shown in neurons that coactivation of the sGC/cGMP pathway converts Sema3A activity from repulsive to attractive (17). Since pericytes contain sGC that is stimulated by NO released from ECs (69), the simultaneous activation of Sema3A and NO/sGC/cGMP signaling could attract pericytes to associate with blood vessels. Along the same lines, it has been recently shown that the creation of perivascular NO gradients in human glioma xenografts increased pericyte coverage and resulted in tumor vessel normalization (70). However, further investigation is needed to clarify the molecular mechanism(s) by which endothelial Sema3A behaves as a chemoattractant for pericytes.

In conclusion, this work unveils what we believe to be a new role of Sema3A as an endogenous antiangiogenic inhibitor that impairs angiogenesis and reduces late-stage tumor volume without inducing enduring hypoxia or interfering with normal vessels. Since reexpression of exogenous Sema3A in tumors induces stable disease and normalizes the vasculature, this molecule holds promise as a target to be considered in designing new and more efficient antiangiogenic and antitumor therapies.

Methods

For experimental procedures not described herein, see Supplemental Methods.

Breeding of transgenic mice. Generation of RipTag2 mice as a model of pancreatic islet cell carcinogenesis has been previously reported (25). RipTag2 mice were maintained on an C57BL/6J background (The Jackson Laboratory). From 12 weeks of age, all RipTag2 mice received 50% sugar food (Harlan Teklad) and 5% sugar water to relieve hypoglycemia induced by the insulin-secreting tumors. Generation of K14-HPV16 transgenic mice (26) and E_2 treatment for cervical carcinogenesis have been previously reported (27, 28). Briefly, 1-month-old virgin female transgenic (heterozygous K14-HPV16) and nontransgenic (FVB/n) mice were anesthetized with 2.5% Avertin, and continuous release pellets that deliver E_2 at doses of 0.05 mg over 60 days (Innovative Research of America Inc.) were implanted s.c. in the dorsal back skin. Subsequent pellets were implanted at 3 and 5 months of age for a total of 6 months of hormone treatment. K14-HPV16 mice were maintained in the FVB/n background (The Jackson Laboratory). Mice were monitored throughout the experiments for complications due to the dysplastic nature of their skin or to the E_2 treatment. RipTag2 mice breeding pairs were provided by D. Hanahan (UCSF, San Francisco, California, USA) and O. Casanovas (Catalan Institute of Oncology, Barcelona, Spain); K14-HPV16 mice were also supplied by D. Hanahan. All animal procedures were approved by the Ethical Commission of the University of Turin and by the Italian Ministry of Health in compliance with international laws and policies.

Immunohistochemical analysis. All immunohistochemical and immunofluorescence analyses were performed as previously described (28, 41) and are detailed in Supplemental Methods. All specimens of human normal cervix, CIN3 lesion, and cervical cancer were provided by K. Smith-McCune (UCSF Comprehensive Cancer Center, San Francisco, California, USA) and obtained as paraffin-embedded sections. These samples derived from different patients (12 different patients per stage) and were obtained from the Department of Pathology archives at UCSF based on the histopathological diagnosis of normal tissue, CIN-3 lesion, and cancer.

AAV vector preparation and viral production. The rAAV vectors used in this study were produced by the AAV Vector Unit at ICGEB Trieste, according to a previously described protocol (36). The AAV vector backbone is based on the pAAV-MCS from Stratagene and was engineered in order to express Sema3A-Myc cDNA and the LacZ gene under control of the constitutive CMV immediate early promoter. The viral stocks used in this study were obtained with titers of 1×10^{12} to 1×10^{13} viral genome particles/ml, using a packaging plasmid encoding the serotype 8 capsid protein (71).

In vivo AAV8 administration. Before treatment, a 5% glucose gavage was performed. Animals were anesthetized with i.p. Avertin (tribromoethanol 250 mg/kg). The superior mesenteric artery was exposed after a displacement of intestine. With a 30-gauge needle (Roboz), 100 μl of AAV8 was injected slowly through the abdominal aorta, which was simultaneously clamped just below the celiac artery, thus reaching the superior pancreatic-duodenal and lienal arteries. After injection, hemostasis was achieved by pressure on the artery. The abdomen was closed layer to layer with 5-0 chromic gut sutures. Animals were monitored during the subsequent hours and allowed to recover 1–2 hours after surgery. Postsurgical analgesia was achieved by buprenorphine (0.1 mg/kg s.c. q12h for 1 day) and antibiotic prophylaxis with ampicillin (150 mg/kg s.c.).

Collagen gel angiogenesis assay. The angiogenesis bioassay was performed as previously described (53, 54). Angiogenic islets were isolated from RipTag2 mice as described in Supplemental Methods and then incubated for 24 hours at 37°C in a 10% CO_2 balanced air incubator, in DMEM containing 0.5% FCS. Bovine capillary ECs (BCEs) were trypsinized and resuspended in DMEM with 10% calf serum. BCEs were mixed at a 1:3 ratio with a chilled type I collagen solution (3 mg/ml; Roche) in DMEM medium containing 0.1N NaOH and 0.2 M HEPES pH 7.3 (final concentration, 2×10^5 cells/ml). Aliquots (250 μl) of the collagen/cell mixture were added into 48-well tissue culture plates. Angiogenic islets were added to each well before the solution was allowed to gel at 37°C. Medium alone (as untreated control), 10 μg/ml neutralizing VEGF Ab (anti-VEGF Ab; Neomarkers), 10 μM Sema3A inhibitor SM-216289 (Sumitomo Pharma Co.), and both SM-216289 and anti-VEGF Ab were added to the collagen/EC/islet mixture. In each experiment, angiogenic islets alone or BCEs alone were added to the collagen mixture as internal control. Culture plates were incubated in a 5% CO_2, balanced air atmosphere and, after 6 days, were observed for EC growth and migration and capillary-like structure formation.

Sema3A inhibitor SM-216289 administration. Osmotic minipumps (model 1002, Alzet) were filled with 0.1 ml of SM-216289 inhibitor diluted in saline to a final concentration of 0.2 mg/ml. Osmotic minipumps were connected to a silastic tube (25 mm length, 1.65 mm external diameter, 0.7 mm inner diameter) and implanted under anesthesia with Avertin (tribromoethanol, 250 mg/kg) s.c. in the right side of abdomen. The tubing was then passed through the muscular wall to reach pancreas, and both minipump and tube were sutured to the abdominal wall. The proximity of the tip of the tube to pancreas was reassessed at sacrifice. We administered SM-216289 (0.25 μl/h, 1.2 μg/day) or saline (for control mice) for 2 weeks (between 8.5 and 10.5 weeks of age). Twelve RipTag2 mice were employed for both SM-216289 and control treatment. SM-216289 was provided by Toru Kimura (Dainippon Sumitomo Pharma Co., Osaka, Japan).

Experimental trials. Standard techniques for quantifying angiogenic islets and tumors and assessing histopathology (28, 41) are described in Supplemental Methods. AAV8-Sema3A treatment started when mice reached the age of 12 weeks and continued until mice were 16 weeks old for the RTs ($n = 12$) or 14 weeks old for the 2-week short RTs ($n = 10$). In the PTs ($n = 12$), RipTag2 mice were treated from 5 to 10.5 weeks of age (41). To generate a survival curve, 12-week-old Rip Tag2 mice were infected with either AAV8-Sema3A ($n = 20$) or AAV8-lacZ ($n = 20$), and their survival was monitored over time. Kaplan-Meier curve and median survival were calculated by GraphPad Prism (version 5.00; GraphPad Software).

Confocal scanning microscopy quantifications. All immunofluorescence images were captured and analyzed by using a Leica TCS SP2 AOBS confocal laser-scanning microscope (Leica Microsystems). Image acquisition was performed maintaining the same laser power, gain, and offset settings. We analyzed 10 different fields for each control or Sema3A-treated mouse. To quantify pericyte coverage (red channel: NG2, SMA, and PDGFR-β) and total or active β_1 integrin (red channel), in each picture we drew a region of interest (ROI) close to each blood vessel (green channel: Meca-32 and CD31). Next, we quantified the mean fluorescence intensity of red and green channels by means of the Leica Confocal Software Histogram Quantification Tool. Then, we calculated the ratio of red to green channel mean fluorescence intensity. Values are expressed as percentage of red to green costaining. To quantify the amount of apoptotic (red channel: cleaved caspase-3) and proliferating (red channel: Ki-67) cells, in each analyzed picture we drew 5 random ROIs of the same size. Then, we calculated the ratio of red to blue (DAPI) channel mean fluorescence intensity. This ratio was expressed as percentage of caspase-3^+ and Ki-67^+ cells relative to total cells.

Analysis of tumor vasculature and vessel branching. Data were obtained from the analysis of 10 controls and 10 Sema3A-treated mice. For each animal, the total vessel area of at least five ×400 power field pictures was quantified by computer-assisted analysis of Meca-32–positive structures present in each tumor section. To this end, we employed Image-Pro Plus 6.2 software (Media Cybernetics). High-resolution confocal image stacks of vessels stained with anti–Meca-32 Ab were reconstructed by isosurface rendering using Imaris software (version 6.2.0; Bitplane AG). Isosurface rendering is a computer-generated representation of a specified range of fluorescence intensities in a data set that allows the creation of an artificial solid object of a specific area. Stacks of RGB color confocal images of RipTag2 tumors stained by immunohistochemistry were imported into Imaris to obtain a precise 3D reconstruction of the vascular network and vessel morphology. Confocal images were processed with the imaging software winRHIZO Pro (Regent Instruments Inc.) to analyze vessel branching and diameter. This software reproduces vessel pattern, identifies vessel branching, and gives back forks (blood vessel branch points) per area. Branching was thus calculated as number of forks relative to total vessel area. Five fields per mouse from a total of 10 mice per treatment group were analyzed.

Hypoxia assay. Hypoxia in tumors was detected by the formation of pimonidazole adducts after tail injection of pimonidazole hydrochloride compound into tumor-bearing animals for 90 minutes. Pancreas sections were immunostained to detect pimonidazole adducts using Hypoxyprobe-1–Mab1 FITC Ab (Hypoxyprobe-1 Plus kit; Chemicon/Millipore) according to the manufacturer's instructions (5).

Statistics. All values are expressed as mean ± SD. For all statistical analyses a 2-tailed, unpaired Mann-Whitney *U* test was performed by using SPSS software version 15.0 (SPSS Inc.). A *P* value less than 0.05 was considered significant. Statistical analysis for Kaplan-Maier survival curve was performed using the log-rank (Mantel-Cox) test.

Acknowledgments

We thank Doug Hanahan for discussion and insightful suggestions on the manuscript and for providing breeding pairs for RipTag2 and K14-HPV16 mouse colonies. We thank Karen Smith-McCune for providing human tissue samples and for useful suggestions on the manuscript. Rakesh K. Jain is gratefully acknowledged for his valuable comments. We thank Oriol Casanovas for supplying

RipTag2 mice and βTC3 cells. We thank Toru Kimura for kindly providing the SM-216289 inhibitor. We thank Serge Masson for his help in the calculation and generation of the Kaplan-Meier curve. This work was supported by the Associazione Italiana per la Ricerca sul Cancro (AIRC) (to E. Giraudo, F. Bussolino, and G. Serini); Fondazione Guido Berlucchi (to E. Giraudo and G. Serini); Associazione Augusto per la Vita (to G. Serini); Regione Piemonte Ricerca Sanitaria Finalizzata 2006, 2007, 2008 (to E. Giraudo, G. Serini, and F. Bussolino), Ricerca Scientifica Applicata 2004 (to E. Giraudo and F. Bussolino), Ricerca Industriale e Sviluppo precompetitivo 2006, grants PRESTO and SPLASERBA (to G. Serini and F. Bussolino), Piattaforme Tecnologiche per le Biotecnologie — Grant Druidi (to F. Bussolino); Fondazione Cassa di Risparmio di Torino — Progetto Alfieri (to F. Bussolino); Ministero della Salute Programma di Ricerca Finalizzata 2006 and Programma Straordinario di Ricerca Oncologica 2006 (to E. Giraudo, F. Bussolino, and G. Serini); Telethon, Italy (to G. Serini).

Received for publication May 24, 2008, and accepted in revised form August 6, 2009.

Address correspondence to: Enrico Giraudo, Laboratory of Transgenic Mouse Models, Division of Vascular Biology, Institute for Cancer Research and Treatment (IRCC), and Department of Oncological Sciences, University of Torino School of Medicine, Strada Provinciale 142, Km 3.95, I-10060 Candiolo, Turin, Italy. Phone: 39-011-9933505; Fax: 39-011-9933524; E-mail: enrico.giraudo@ircc.it.

1. Folkman, J. 2006. Angiogenesis. *Annu. Rev. Med.* **57**:1–18.
2. Jain, R.K. 2005. Normalization of tumor vasculature: an emerging concept in antiangiogenic therapy. *Science.* **307**:58–62.
3. Inoue, M., Hager, J.H., Ferrara, N., Gerber, H.P., and Hanahan, D. 2002. VEGF-A has a critical, nonredundant role in angiogenic switching and pancreatic beta cell carcinogenesis. *Cancer Cell.* **1**:193–202.
4. Jain, R.K., Duda, D.G., Clark, J.W., and Loeffler, J.S. 2006. Lessons from phase III clinical trials on anti-VEGF therapy for cancer. *Nat. Clin. Pract. Oncol.* **3**:24–40.
5. Casanovas, O., Hicklin, D.J., Bergers, G., and Hanahan, D. 2005. Drug resistance by evasion of antiangiogenic targeting of VEGF signaling in late-stage pancreatic islet tumors. *Cancer Cell.* **8**:299–309.
6. Fischer, C., et al. 2007. Anti-PlGF inhibits growth of VEGF(R)-inhibitor-resistant tumors without affecting healthy vessels. *Cell.* **131**:463–475.
7. Winkler, F., et al. 2004. Kinetics of vascular normalization by VEGFR2 blockade governs brain tumor response to radiation: role of oxygenation, angiopoietin-1, and matrix metalloproteinases. *Cancer Cell.* **6**:553–563.
8. Carmeliet, P., and Tessier-Lavigne, M. 2005. Common mechanisms of nerve and blood vessel wiring. *Nature.* **436**:193–200.
9. Bussolino, F., Valdembri, D., Caccavari, F., and Serini, G. 2006. Semaphoring Vascular Morphogenesis. *Endothelium.* **13**:81–91.
10. Serini, G., et al. 2003. Class 3 semaphorins control vascular morphogenesis by inhibiting integrin function. *Nature.* **424**:391–397.
11. Bielenberg, D.R., Pettaway, C.A., Takashima, S., and Klagsbrun, M. 2006. Neuropilins in neoplasms: expression, regulation, and function. *Exp. Cell Res.* **312**:584–593.
12. Kessler, O., et al. 2004. Semaphorin-3F is an inhibitor of tumor angiogenesis. *Cancer Res.* **64**:1008–1015.
13. Kaneko, S., et al. 2006. A selective Sema3A inhibitor enhances regenerative responses and functional recovery of the injured spinal cord. *Nat. Med.* **12**:1380–1389.
14. Vacca, A., et al. 2006. Loss of inhibitory semaphorin 3A(SEMA3A) autocrine loops in bone marrow endothelial cells of patients with multiple myeloma. *Blood.* **108**:1661–1667.
15. Guttmann-Raviv, N., et al. 2007. Semaphorin-3A and semaphorin-3F work together to repel endothelial cells and to inhibit their survival by induction of apoptosis. *J. Biol. Chem.* **282**:26294–26305.
16. Acevedo, L.M., Barillas, S., Weis, S.M., Gothert, J.R., and Cheresh, D.A. 2008. Semaphorin 3A suppresses VEGF-mediated angiogenesis yet acts as a vascular permeability factor. *Blood.* **111**:2674–2680.
17. Zhou, Y., Gunput, R.A., and Pasterkamp, R.J. 2008. Semaphorin signaling: progress made and promises ahead. *Trends Biochem. Sci.* **33**:161–170.
18. Narazaki, M., and Tosato, G. 2006. Ligand-induced internalization selects use of common receptor neuropilin-1 by VEGF165 and semaphorin3A. *Blood.* **107**:3892–3901.
19. Damon, D.H. 2006. Vascular endothelial-derived semaphorin 3 inhibits sympathetic axon growth. *Am. J. Physiol. Heart Circ. Physiol.* **290**:H1220–H1225.
20. Ito, T., et al. 2000. Repulsive axon guidance molecule Sema3A inhibits branching morphogenesis of fetal mouse lung. *Mech. Dev.* **97**:35–45.
21. Kigel, B., Varshavsky, A., Kessler, O., and Neufeld, G. 2008. Successful inhibition of tumor development by specific class-3 semaphorins is associated with expression of appropriate semaphorin receptors by tumor cells. *PLoS ONE.* **3**:e3287.
22. Christensen, C., et al. 2005. Proteolytic processing converts the repelling signal Sema3E into an inducer of invasive growth and lung metastasis. *Cancer Res.* **65**:6167–6177.
23. Rolny, C., et al. 2008. The tumor suppressor semaphorin 3B triggers a prometastatic program mediated by interleukin 8 and the tumor microenvironment. *J. Exp. Med.* **205**:1155–1171.
24. Hanahan, D., and Folkman, J. 1996. Patterns and emerging mechanisms of the angiogenic switch during tumorigenesis. *Cell.* **86**:353–364.
25. Hanahan, D. 1985. Heritable formation of pancreatic beta-cell tumours in transgenic mice expressing recombinant insulin/simian virus 40 oncogenes. *Nature.* **315**:115–122.
26. Coussens, L.M., Hanahan, D., and Arbeit, J.M. 1996. Genetic predisposition and parameters of malignant progression in K14-HPV16 transgenic mice. *Am. J. Pathol.* **149**:1899–1917.
27. Arbeit, J.M., Howley, P.M., and Hanahan, D. 1996. Chronic estrogen-induced cervical and vaginal squamous carcinogenesis in human papillomavirus type 16 transgenic mice. *Proc. Natl. Acad. Sci. U. S. A.* **93**:2930–2935.
28. Giraudo, E., Inoue, M., and Hanahan, D. 2004. An amino-bisphosphonate targets MMP-9-expressing macrophages and angiogenesis to impair cervical carcinogenesis. *J. Clin. Invest.* **114**:623–633.
29. Bergers, G., Javaherian, K., Lo, K.M., Folkman, J., and Hanahan, D. 1999. Effects of angiogenesis inhibitors on multistage carcinogenesis in mice. *Science.* **284**:808–812.
30. Guttmann-Raviv, N., et al. 2006. The neuropilins and their role in tumorigenesis and tumor progression. *Cancer Lett.* **231**:1–11.
31. Herzog, Y., Kalcheim, C., Kahane, N., Reshef, R., and Neufeld, G. 2001. Differential expression of neuropilin-1 and neuropilin-2 in arteries and veins. *Mech. Dev.* **109**:115–119.
32. Toyofuku, T., et al. 2004. Dual roles of Sema6D in cardiac morphogenesis through region-specific association of its receptor, Plexin-A1, with off-track and vascular endothelial growth factor receptor type 2. *Genes Dev.* **18**:435–447.
33. Roodink, I., et al. 2005. Plexin D1 expression is induced on tumor vasculature and tumor cells: a novel target for diagnosis and therapy? *Cancer Res.* **65**:8317–8323.
34. Smith-McCune, K., Zhu, Y.H., Hanahan, D., and Arbeit, J. 1997. Cross-species comparison of angiogenesis during the premalignant stages of squamous carcinogenesis in the human cervix and K14-HPV16 transgenic mice. *Cancer Res.* **57**:1294–1300.
35. Park, K., et al. 2008. Cancer gene therapy using adeno-associated virus vectors. *Front. Biosci.* **13**:2653–2659.
36. Wang, Z., et al. 2006. Widespread and stable pancreatic gene transfer by adeno-associated virus vectors via different routes. *Diabetes.* **55**:875–884.
37. Shirvan, A., et al. 1999. Semaphorins as mediators of neuronal apoptosis. *J. Neurochem.* **73**:961–971.
38. Bagnard, D., et al. 2004. Differential MAP kinases activation during semaphorin3A-induced repulsion or apoptosis of neural progenitor cells. *Mol. Cell. Neurosci.* **25**:722–731.
39. Paez-Ribes, M., et al. 2009. Antiangiogenic therapy elicits malignant progression of tumors to increased local invasion and distant metastasis. *Cancer Cell.* **15**:220–231.
40. Armulik, A., Abramsson, A., and Betsholtz, C. 2005. Endothelial/pericyte interactions. *Circ. Res.* **97**:512–523.
41. Bergers, G., Song, S., Meyer-Morse, N., Bergsland, E., and Hanahan, D. 2003. Benefits of targeting both pericytes and endothelial cells in the tumor vasculature with kinase inhibitors. *J. Clin. Invest.* **111**:1287–1295.
42. Willett, C.G., et al. 2004. Direct evidence that the VEGF-specific antibody bevacizumab has antivascular effects in human rectal cancer. *Nat. Med.* **10**:145–147.
43. Hamzah, J., et al. 2008. Vascular normalization in Rgs5-deficient tumours promotes immune destruction. *Nature.* **453**:410–414.
44. Yamagishi, H., Olson, E.N., and Srivastava, D. 2000. The basic helix-loop-helix transcription factor, dHAND, is required for vascular development. *J. Clin. Invest.* **105**:261–270.
45. Hynes, R.O. 2002. A reevaluation of integrins as regulators of angiogenesis. *Nat. Med.* **8**:918–921.
46. Serini, G., Valdembri, D., and Bussolino, F. 2006. Integrins and angiogenesis: a sticky business. *Exp. Cell Res.* **312**:651–658.
47. Parsons-Wingerter, P., et al. 2005. Uniform overexpression and rapid accessibility of alpha5beta1 integrin on blood vessels in tumors. *Am. J. Pathol.* **167**:193–211.
48. Lenter, M., et al. 1993. A monoclonal antibody against an activation epitope on mouse integrin chain beta 1 blocks adhesion of lymphocytes to the endothelial integrin alpha 6 beta 1. *Proc. Natl. Acad. Sci. U. S. A.* **90**:9051–9055.

49. Bazzoni, G., Shih, D.T., Buck, C.A., and Hemler, M.E. 1995. Monoclonal antibody 9EG7 defines a novel beta 1 integrin epitope induced by soluble ligand and manganese, but inhibited by calcium. *J. Biol. Chem.* **270**:25570–25577.
50. Valentijn, A.J., Zouq, N., and Gilmore, A.P. 2004. Anoikis. *Biochem. Soc. Trans.* **32**:421–425.
51. Abraham, S., Kogata, N., Fassler, R., and Adams, R.H. 2008. Integrin {beta}1 Subunit Controls Mural Cell Adhesion, Spreading, and Blood Vessel Wall Stability. *Circ. Res.* **102**:562–570.
52. Kikuchi, K., et al. 2003. In vitro and in vivo characterization of a novel semaphorin 3A inhibitor, SM-216289 or xanthofulvin. *J. Biol. Chem.* **278**:42985–42991.
53. Folkman, J., Watson, K., Ingber, D., and Hanahan, D. 1989. Induction of angiogenesis during the transition from hyperplasia to neoplasia. *Nature.* **339**:58–61.
54. Bergers, G., et al. 2000. Matrix metalloproteinase-9 triggers the angiogenic switch during carcinogenesis. *Nat. Cell Biol.* **2**:737–744.
55. Bielenberg, D.R., et al. 2004. Semaphorin 3F, a chemorepulsant for endothelial cells, induces a poorly vascularized, encapsulated, nonmetastatic tumor phenotype. *J. Clin. Invest.* **114**:1260–1271.
56. Bielenberg, D.R., and Klagsbrun, M. 2007. Targeting endothelial and tumor cells with semaphorins. *Cancer Metastasis Rev.* **26**:421–431.
57. Joyce, J.A., et al. 2003. Stage-specific vascular markers revealed by phage display in a mouse model of pancreatic islet tumorigenesis. *Cancer Cell.* **4**:393–403.
58. Hoffman, J.A., et al. 2003. Progressive vascular changes in a transgenic mouse model of squamous cell carcinoma. *Cancer Cell.* **4**:383–391.
59. Ryschich, E., et al. 2006. Molecular fingerprinting and autocrine growth regulation of endothelial cells in a murine model of hepatocellular carcinoma. *Cancer Res.* **66**:198–211.
60. Neufeld, G., and Kessler, O. 2008. The semaphorins: versatile regulators of tumour progression and tumour angiogenesis. *Nat. Rev. Cancer.* **8**:632–645.
61. Futamura, M., et al. 2007. Possible role of semaphorin 3F, a candidate tumor suppressor gene at 3p21.3, in p53-regulated tumor angiogenesis suppression. *Cancer Res.* **67**:1451–1460.
62. Hanson, J.A., et al. 2006. Gene promoter methylation in prostate tumor-associated stromal cells. *J. Natl. Cancer Inst.* **98**:255–261.
63. Shih, T., and Lindley, C. 2006. Bevacizumab: an angiogenesis inhibitor for the treatment of solid malignancies. *Clin. Ther.* **28**:1779–1802.
64. Fischer, C., Mazzone, M., Jonckx, B., and Carmeliet, P. 2008. FLT1 and its ligands VEGFB and PlGF: drug targets for anti-angiogenic therapy? *Nat. Rev. Cancer.* **8**:942–956.
65. Pan, Q., et al. 2007. Blocking neuropilin-1 function has an additive effect with anti-VEGF to inhibit tumor growth. *Cancer Cell.* **11**:53–67.
66. Stoeltzing, O., et al. 2003. Inhibition of integrin alpha5beta1 function with a small peptide (ATN-161) plus continuous 5-FU infusion reduces colorectal liver metastases and improves survival in mice. *Int. J. Cancer.* **104**:496–503.
67. Kim, S., Bakre, M., Yin, H., and Varner, J.A. 2002. Inhibition of endothelial cell survival and angiogenesis by protein kinase A. *J. Clin. Invest.* **110**:933–941.
68. Song, S., Ewald, A.J., Stallcup, W., Werb, Z., and Bergers, G. 2005. PDGFRbeta+ perivascular progenitor cells in tumours regulate pericyte differentiation and vascular survival. *Nat. Cell Biol.* **7**:870–879.
69. Cary, S.P., Winger, J.A., Derbyshire, E.R., and Marletta, M.A. 2006. Nitric oxide signaling: no longer simply on or off. *Trends Biochem. Sci.* **31**:231–239.
70. Kashiwagi, S., et al. 2008. Perivascular nitric oxide gradients normalize tumor vasculature. *Nat. Med.* **14**:255–257.
71. Gao, G.P., et al. 2002. Novel adeno-associated viruses from rhesus monkeys as vectors for human gene therapy. *Proc. Natl. Acad. Sci. U. S. A.* **99**:11854–11859.